

AMERICAN UNIVERSITY OF BEIRUT

ANALYSIS OF A MOBILE ROBOT WITH AN ANGULAR
SWIVEL STEERING MECHANISM WITH
APPLICATIONS TO STEP CLIMBING

by

Wael Ahmad Salem

A thesis
submitted in partial fulfillment of the requirements
for the degree of Master of Engineering
to the Department of Mechanical Engineering
of the Faculty of Engineering and Architecture
at the American University of Beirut

Beirut, Lebanon
May 2014

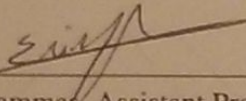
AMERICAN UNIVERSITY OF BEIRUT

ANALYSIS OF A MOBILE ROBOT WITH AN ANGULAR
SWIVEL STEERING MECHANISM WITH
APPLICATIONS TO STEP CLIMBING

by

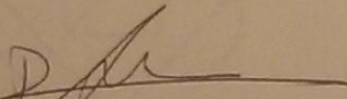
Wael Ahmad Salem

Approved by:



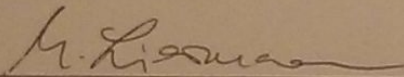
Elie Shamma, Assistant Professor
Mechanical Engineering

Advisor



Daniel Asmar, Assistant Professor
Mechanical Engineering

Committee Member



Matthias Liermann, Assistant Professor
Mechanical Engineering

Committee Member

Date of thesis defense: 06/05/2014

AMERICAN UNIVERSITY OF BEIRUT

THESIS, DISSERTATION, PROJECT RELEASE FORM

Student Name: Salem Wael Ahmad
Last First Middle

Master's Thesis Master's Project Doctoral Dissertation

I authorize the American University of Beirut to: (a) reproduce hard or electronic copies of my thesis, dissertation, or project; (b) include such copies in the archives and digital repositories of the University; and (c) make freely available such copies to third parties for research or educational purposes.

I authorize the American University of Beirut, **three years after the date of submitting my thesis, dissertation, or project**, to: (a) reproduce hard or electronic copies of it; (b) include such copies in the archives and digital repositories of the University; and (c) make freely available such copies to third parties for research or educational purposes.

Wael 19/5/2014
Signature Date

This form is signed when submitting the thesis, dissertation, or project to the University Libraries

ACKNOWLEDGEMENTS

I would like to thank my supervisor, Professor Elie Shammas, for the advise and guidance he provided throughout my time as a graduate student. I was lucky to have an advisor who cared for my work, and who was always there for support. I would also like to thank the member of my thesis committee, Prof Matthias Liermann and Prof Daniel Asmar, who provided me with enough support and information to make this project possible.

I would like to express thanks to my family, who were always there to support me no matter how difficult things got. They were always prepared to give me morale and comfort me during the long night of work and research. Completing this work would not have been possible without the support of my peers and friends.

Finally, I would like to thank the American University of Beirut, the University Research Board at the American University of Beirut and by the Lebanese National Council for Scientific Research without whom the project would not have been complete.

AN ABSTRACT OF THE THESIS OF

Wael Ahmad Salem for Master of Engineering
Major: Mechanical Engineering

Title: Analysis of a Mobile Robot with an Angular Swivel Steering Mechanism with Applications to Step Climbing

The use of wheeled mobile robots in human environments is increasing rapidly. Many robots that are capable of navigating rough terrains have been proposed in literature. However, these have complex methods of actuation and are difficult to build. In this paper, we present the swivel car: a simple mobile platform with an active angular swivel steering mechanism that provides it with the ability to navigate through human environments. In particular, this robot demonstrates step climbing capabilities that prove to be useful in human environments. To study these capabilities, we create various kinematic and dynamic models. These models are used as a basis for comparison with other mobile robots of similar dimensions to determine the effectiveness of its climbing capabilities. These models are obtained by making simplifying assumptions to reduce the complexity of the mobile robot.

CONTENTS

	Page
AKNOWLEDGEMENTS	v
ABSTRACT	vi
Contents	vii
LIST OF ILLUSTRATIONS	ix
ILLUSTRATIONS	ix
LIST OF TABLES	xiii
Chapter	
I. Introduction	1
1. Related Work	1
2. Thesis Contribution	6
II. Design and Analysis of the Swivel Car	8
A. Preliminary Design	8
B. Kinematic Analysis	10
1. DH Parameters and End-Effector Position	12
2. Lift Constraint	14
3. Point of Contact Analysis	16
4. Steering Capabilities	18
5. Step Climbing Kinematics of the swivel car	21
C. Dynamics of the Steering Mechanism	25

1. Dynamic Analysis of the Steering Mechanism	26
2. Cost of Climbing a Step	28
3. Dependency of Peak Torque on h	29
D. Platform Model with Nonholonomic Constraints	30
1. Nonholonomic Constraints	30
2. Platform Model	32
3. Effects of Varying Model Parameters	38
E. Planar Motion Kinematics	39
F. Parameter Study	43
1. Rules of Thumb for Parameter Selection	44
2. Effects of Varying The Design Parameters	45
a. The Angle ϕ	45
b. Steering Wheel Shaft Length	46
c. "T" Column Length	46
III. Step Climbing Algorithm	47
A. For a Positive ϕ	47
B. For a Negative ϕ	50
1. Force Analysis for Procedure	51
2. Kinematic Analysis of the Step Climbing Process	55
IV. Comparison to Other Mobile Platforms	61
A. Normal Vehicles	61
B. Other Mobile Robots with Climbing Capabilities	64
V. Conclusion	66
Bibliography	67

ILLUSTRATIONS

Figure		Page
1.	A wheeled leg from the robot Hylos	2
2.	The Octopus Robot with labeled parts	3
3.	Step climbing process of the Octopus robot	3
4.	The Rocky 7 rover moving about in rough terrain	3
5.	The hybrid robot MHT moving on flat terrain	4
6.	A complete model of the mobile robot WheelLeg	5
7.	The six-wheeled mobile robot SHRIMP developed in EPFL	5
8.	Genbu climbing over a small step using the passive swivel joint	6
9.	A simple model of the swivel car in Webots	7
10.	Proposed design of the swivel car	9
11.	Proposed design for the internal body of the swivel car	9
12.	A section view of the differential housing showing the differential, the shafts used to move the wheels, and bearing that support the shafts.	10
13.	Section view of the swivel car design	10
14.	The simplified robotic model of the swivel car used to determine the DH parameters of the proposed mobile base.	11
15.	The change in the swivel car configuration for a position ϕ ,(a), and a negative ϕ , (b).	12

16.	Skeletal representation of the swivel car along with the labeled frames and axes.	13
17.	The steering wheel configuration and the direction of its steering axis with respect to the O_0 frame.	14
18.	The effects of varying ϕ on the lift constraint. The figure to the left depicts this variation for positive values of ϕ , whereas the figure on the right depicts this relationship for a negative ϕ	16
19.	The effects of changing the sign of ϕ on the motion of the front steering wheel.	16
20.	Four frames illustrating the path of p in the XZ plane as θ_2 varies from 0 to $\frac{\pi}{2}$ for $l=20$ cm, $h=10$ cm, $\phi = \frac{\pi}{6}$ and $r=0.33$ cm	18
21.	Steering angle versus the change in the twist angle, θ_2 , for different values of the design parameter ϕ	19
22.	Change in the steering kinematics of the mobile base for a positive(left) and negative(right) value of ϕ	20
23.	Sketch of the wheel showing the location of P_r and P_L with respect to an inertial frame O_0	22
24.	Height variation of the random point P_r about the circumference of the lifted wheel for different values of θ_2	23
25.	The height of the lowest point, P_l , as a function of the swivel angle, θ_2	23
26.	Change of step climbing capabilities as ϕ varies	24
27.	The effect of changing the wheel shaft length , h , on the maximum scalable step	24
28.	The effect of changing the length of “T” column, l on the maximum scalable step.	25
29.	The effect of changing the wheel radius, r , on the maximum scalable step.	25

30.	The swivel car climbing an obstacle by actuating the swivel joint, which also acts as its steering mechanism	28
31.	A graph showing the expended energy during a step climbing process, along with the peak torque as the swivel angle changes	29
32.	A plot depicting the change peak torque at the swivel joint to climb a step versus the increase in h	30
33.	A single wheel as seen from above with its nonholonomic constraints. . .	31
34.	Simplified swivel car model with nonholonomic constraints modeled as a 2D planar mechanism	33
35.	Changes in the input for u , v , and α versus the variation of the swivel joint	36
36.	Input to each joint along with the output.	37
37.	Change in pose of the swivel car starting from initial position, (a), and the final position of the swivel car when θ_2 reaches $\frac{\pi}{2}$, (d).	37
38.	The effect of actuating the swivel joint on the position ,x and y, and the orientation θ	38
39.	The simplified planar model of the swivel car resembles that of a tricycle with a variable offset steering wheel.	39
40.	The path followed by solving the equations of motion (67) and (68). . . .	43
41.	A simple representation of the swivel at its initial position and at the position just before the mobile base tips over	44
42.	A simple representation of the swivel car along with its steering shaft at a twist angle of $\frac{\pi}{2}$	45
43.	The swivel car positioning itself to climb a step	48
44.	Variables taken into account during the step climbing process	50
45.	Implementation of the step climbing procedure	50

46.	A skeletal diagram representing the forces and torques about the swivel joint when the front wheel is in contact with a step.	51
47.	A free body diagram showing the forces acting on the swivel car.	52
48.	Driving torque, τ_D , versus induced torque, τ_S for $h = (1, 2, 3, 4, 5)$	53
49.	Driving torque, τ_D , versus induced torque, τ_S for $h = (0.5, 0.7, 0.9, 1.1, 1.3)$	53
50.	Induced torque, τ_S , vs. the change in the swivel angle, θ_2 for $h = (0.5, 0.7, 0.9, 1.1, 1.3)$	54
51.	Induced torque, τ_S , vs. the change in the swivel angle, θ_2 , for $h = (0.5, 0.7, 0.9, 1.1, 1.3)$	54
52.	Approach angle α_{AP}	55
53.	Skeletal representation of the swivel car showing the intersection of the step's surface with the plane formed by the two points, C_F and P_L	56
54.	Change in position of P_L in the XZ plane when θ_2 varies from 0 to $\frac{\pi}{2}$	57
55.	Change in position of C_F in the XZ plane when θ_2 varies from 0 to $\frac{\pi}{2}$	58
56.	Change in position of P_L and C_F in the XZ plane with respect to the origin O_0	59
57.	Minimum value required for the approach angle to overcome a step without interference from the steering wheel.	60
58.	Minimum value required for the approach angle to overcome a step of certain height, without interference from the steering wheel.	60
59.	The crank-slider mechanism used to model the climbing process of a car-like robot	62
60.	Torque variation with time of the step climbing process	64
61.	Energy consumption of the step climbing process vs. time	64

TABLES

Table		Page
1.	DH parameters for the first design	12
2.	Simulation parameters	23
3.	Effects of changing the design parameters on the robot's motion	38
4.	Simulation parameters for car-like robot	63

CHAPTER I

INTRODUCTION

Most mobile platforms, such as differential-driven robots [1] and car-like robots [2], possess limited or no step climbing capabilities unless a mechanism that facilitates step climbing is appended [3]. Vehicles with no, or limited, climbing capabilities are referred to as classical vehicles. While navigating rough terrains or human environments, a wheeled robot is bound to encounter a step and, if the step height is greater than the wheel radius, the robot is forced to find a different path to reach its destination. Recomputing the path will require complex path planning and navigation algorithms, and sometimes an alternative path might not exist. It would be much easier if the robot was able to climb over the obstacle.

1. Related Work

To avoid complex path planning and navigation algorithms, numerous mobile robots with step climbing capabilities have been proposed in literature [3, 4, 6]. These robots are capable of climbing steps of heights larger than the wheel radius, but in turn require complex control algorithms to perform this maneuver. Some of the proposed designs, such as Hylos [4, 5] and MHT [6, 7], use active wheel-legs to climb steps and obstacles. These robots are referred to as hybrid robots because they combine the mobility of the wheel and the climbing capabilities of legs. Such a combination allows for easy and efficient locomotion in flat terrain, and for leg-like climbing motion in rough terrain. The hybrid robot MHT demonstrates impressive obstacle scaling capabilities and can easily navigate through rough terrain. However, to achieve this, the robot requires fourteen degrees of freedom. Furthermore, due to the complexity of this

design, complicated control algorithms are needed to scale obstacles and maintain a stable robot posture at the same time. Fig. 1 shows a wheel-leg taken from Hylos, notice the complexity and required mechanism to construct and actuate a single one of these mechanisms.

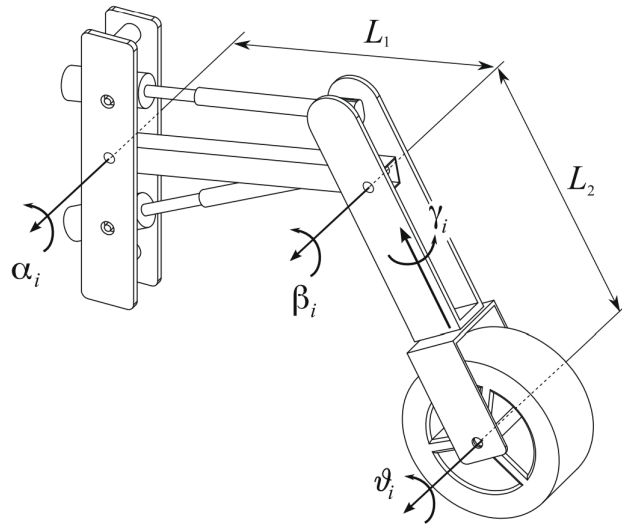


Figure 1: A wheeled leg from the robot Hylos

The mobile robot Octopus [8], shown in Fig. 2, is an eight wheeled robot with fifteen degrees of freedom. The robot is 43 cm long, 42 cm wide, 23 cm high, and weighs 10 kg. As illustrated in Fig. 3, Octopus can use the tactile wheels located at the end of its forearms to climb steps almost twice as large as its wheel diameter. Though effective when climbing large obstacles and scaling steps, this mobile robot is complicated to manufacture and control. It has fifteen degrees of freedom and eight wheels, which is four wheels and ten degrees of freedom more than our model. Furthermore, Octopus requires the use of special tactile wheels with embedded infrared sensors further complicating the design.

The planetary explorer Rocky 7 [9], shown in Fig. 4, employs a rocker-boogie mechanism to climb obstacles and move through rough terrains. Even though it can climb obstacles 50 percent larger than its wheel diameter, the robot's steering capabilities are somewhat limited. Rocky 7 is unable to rotate without moving either forwards or backwards. This can be problematic when navigating in tight or small spaces.



Figure 2: The Octopus Robot with labeled parts

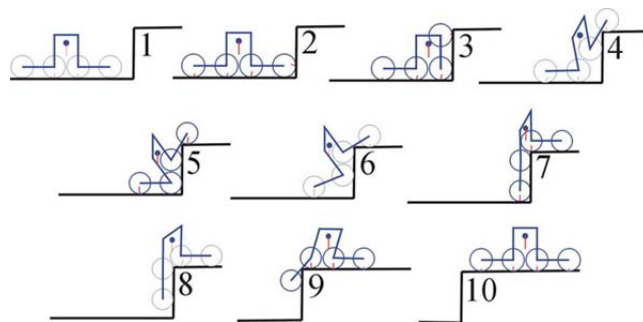


Figure 3: Step climbing process of the Octopus robot



Figure 4: The Rocky 7 rover moving about in rough terrain

MHT is a hybrid mobile robot with twelve degrees of freedom. It was developed for navigation of rough terrains and obstacle climbing. Each leg is composed of two joints and a wheel as seen in Fig. 5. The two joints can lift the wheel over obstacles, and move the robot about rugged terrains similar to a human leg. Unlike the swivel car, MHT was built for military purposes and reconnaissance. Consequently, it is

larger and heavier than our proposed model. It weights almost 150 kg, is almost one meter long and 50 cm wide.



Figure 5: The hybrid robot MHT moving on flat terrain

The mobile robot WheelLeg [13], shown in Fig. 6, is another example of a hybrid robot. Unlike MHT, WheelLeg was constructed with two pneumatically actuated legs at the front and two differential driven wheels at the rear. Each leg is pneumatically actuated with three degrees of freedom and the two rear wheels are independently driven by two motors. This platform was designed to navigate in rough environments which are considered difficult for regular wheeled robots but not so hard to require legged motion. The robot is 111 cm long, 66 cm wide, 40 cm high and weighs almost 25 kg. Due to its design, the robot can be unstable when climbing obstacles, might face traction problems if its front legs are not properly actuated and requires a complex control algorithm to coordinate motion between its legs and wheels when climbing obstacles. Furthermore, this robot requires almost eight controllers to execute its climbing motion and four pneumatic on/off valves to control the motion of each leg. Finally, a pneumatic cylinder is integrated into each leg to achieve the leg-like climbing motion. Using this pneumatic mechanism, WheelLeg can climb obstacles 30 cm high.

Alternatively, robots with passive joints and mechanisms have been developed and implemented as a simple solution to the step climbing problem. Developed in EPFL, shown in Fig. 7, SHRIMP [10] is a six wheel-driven mobile platform weighing almost

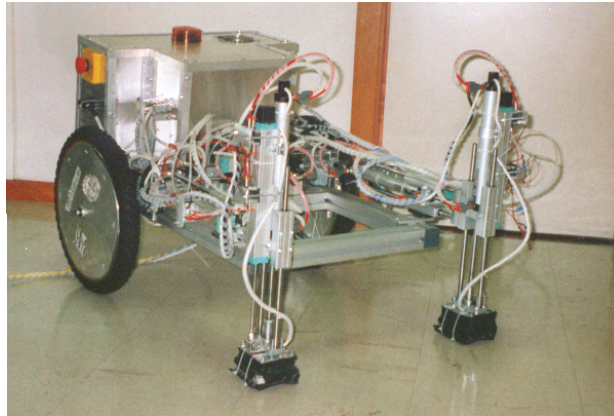


Figure 6: A complete model of the mobile robot WheelLeg

3.1 kg and capable of climbing steps twice as large as its wheel diameter. The body was developed using parallel suspension architecture, allowing the robot to smoothly overcome obstacles and navigate rough terrains with minimal motor power. The wheeled snake robot, Genbu [11, 12], is another example of an active wheel and passive mechanism robot. This mobile robot, shown in Fig. 8, is composed of several wheeled modules connected to each other by passive links. The resulting configuration is a snake robot with high mobility, and an ability to climb steps 10 percent larger than the wheel diameter.

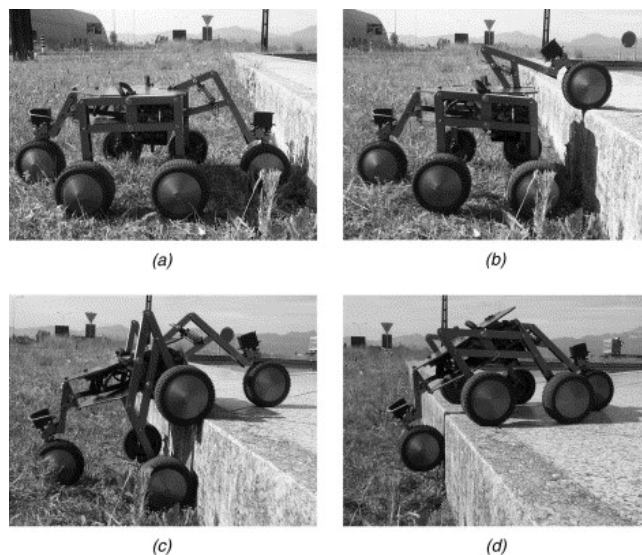


Figure 7: The six-wheeled mobile robot SHRIMP developed in EPFL



Figure 8: Genbu climbing over a small step using the passive swivel joint

2. Thesis Contribution

Our goal is to develop a mobile platform with the following properties: a relatively simple mechanical design, a minimal number of joints and actuators and capability of reaching large steering angles. In [14] we introduced the swivel car, a four-wheeled mobile platform with step climbing capabilities. The design is relatively simple and utilizes only two actuators. Unlike many proposed designs, the swivel car's step climbing capabilities do not depend on the wheel diameter but rather on the length of the wheel shaft. Consequently, it is possible to design a mobile robot with small wheels but with the ability to climb steps larger than the robot itself. Moreover, the swivel car combines two distinct designs that of the classical car-like robot, and that of the wheeled snake robots such as Genbu. Unlike Genbu, the swivel car is designed with active joints, rather than passive, connecting only two modules. This novel design can negotiate rough terrains, climb relatively large obstacles and turn without changing its position. A skeletal design of this mobile base is shown in Fig. 9. The wheel shaft, labeled *A*, rotates about the axis of the swivel joint, labeled *B*. The proposed mobile base does not only possess excellent steering capabilities, it can use this motion to climb steps and obstacles.

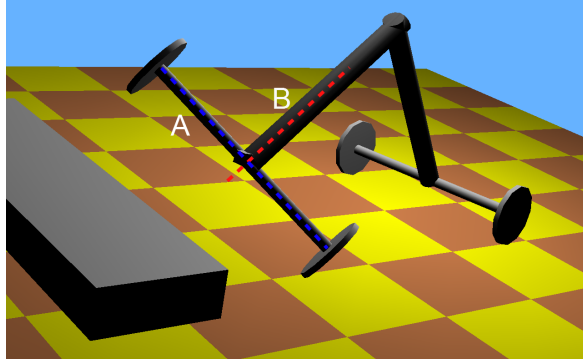


Figure 9: A simple model of the swivel car in Webots

The thesis is divided as follows, a thorough kinematic and dynamic analysis of the car is presented in Section II. In Section III, we compare the step climbing capabilities of our mobile platform to a car-like robot and other step climbing robots of similar size. Finally, we devise a step climbing algorithm in Section IV based on the kinematic and dynamic analysis conducted in Section II.

CHAPTER II

DESIGN AND ANALYSIS OF THE SWIVEL CAR

In this section, we study the dynamics and kinematics of the swivel car. We first present a preliminary design for this mobile platform based on the skeletal configuration shown in Fig. 9. We then analyze the steering capabilities of the platform and the path followed by the motion of the point of contact with respect to a fixed ordinate frame. Next we study the dynamics of the steering mechanism to determine the peak torque requirements of the swivel car, and the energy consumed while steering. This information is used to determine the total energy consumed while climbing a step of certain height. Finally, we devise a simplified platform model to study the effects of actuating the swivel joint on the pose of the swivel car. Using the simplified model, we create a kinematic model to study the motion of the swivel car in a two dimensional plane.

A. Preliminary Design

Now, we present a mechanical design for the platform that was introduced in [14]. The proposed design is comprised of two “T”-shaped bodies joined together at the base of the “T” as seen in Fig. 10. Each of the “T” bodies connect to a central body via two concentric shafts. The inner shaft is the drive shaft that turns the wheel via a differential, shown in Fig. 10, while the outer shaft rotates the entire “T” shaped body. Rotating the entire “T”-shaped body raises one of the wheels above the ground plane, thus allowing for step climbing. The angle about which the “T” column rotates is referred to as the twist(swivel) angle, and is represented by θ_2 throughout this thesis.

Accordingly, the central body houses steering and driving actuators as depicted

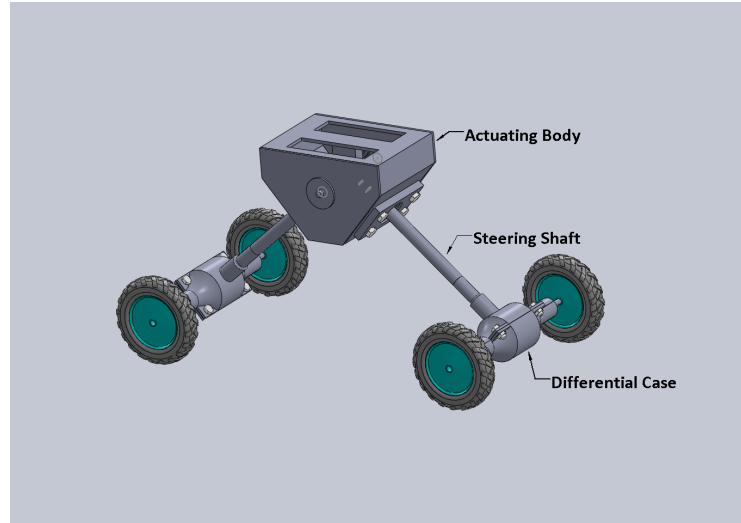


Figure 10: Proposed design of the swivel car

in Fig. 11. The large gear labeled “Steering Gear” is used to move the large steering shaft by rotating the smaller gear located at the sides. The over gear labeled the “Driving Gear” delivers power to the differential shown in Fig. 12, which in turn delivers the power to the wheels. All the other components of the mobile platform, such as batteries, controllers, and electronics, could be housed on or inside the central body. Actuation of the swivel joint is achieved by rotating the steering shaft. In order to actuate the wheels and swivel angle simultaneously, the driving shaft is housed inside the hollow steering shafts as presented in Fig. 13. Both shafts are actuated directly from the central body, and can be moved together or independently.

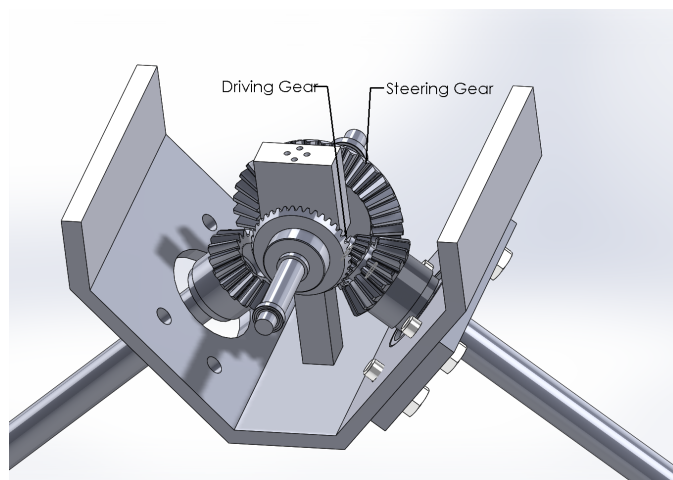


Figure 11: Proposed design for the internal body of the swivel car

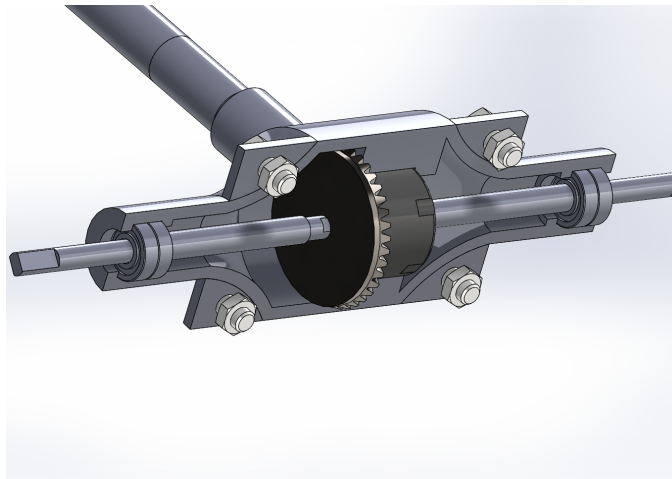


Figure 12: A section view of the differential housing showing the differential, the shafts used to move the wheels, and bearing that support the shafts.

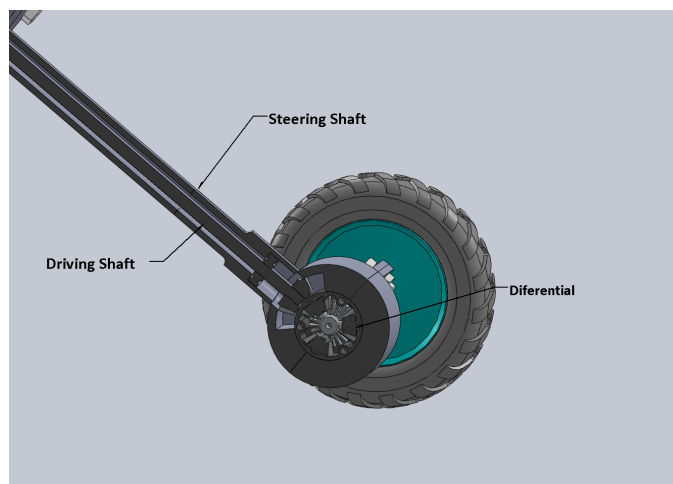


Figure 13: Section view of the swivel car design

Compared to other mobile platforms, this design is relatively easy to operate. Using two actuators, it is possible to drive all four wheels and the swivel joint. However, this design does not leave much room to mount sensors and other attachments.

B. Kinematic Analysis

We now proceed to model and study the kinematic behavior of the swivel car when the twist joint, θ_2 , is actuated. Using this analysis, we determine the steering capabilities of the swivel car, the motion of the steering wheel relative to a fixed frame

and the platform's step climbing capabilities. We begin by analyzing the kinematics of this platform by modeling the swivel car as robotic linkage with two revolute joints, θ_1 and θ_2 , as shown in Fig. 14. The ground frame, O_0 is placed at the center of the rear wheel axis with its z_0 axis pointing along the axis of the rear wheels. The parameters (l, r, ϕ, h) are the dimensions of the robot. This simplification allows us to determine the platform's steering capabilities through simple kinematics transformations, as well as the motion of its steering wheel with respect to a fixed frame. This analysis is performed for different configurations of the swivel car, which are achieved by varying the parameter ϕ from $-\frac{\pi}{2} + \frac{\pi}{12}$ to $\frac{\pi}{2} - \frac{\pi}{12}$. Throughout this analysis, we notice a significant change in the platform's kinematic behavior once ϕ changes sign from negative to positive. Fig. 15 shows the difference between the two aforementioned configurations. Notice when ϕ is negative, the shaft of the "T" column actually penetrates the ground. This means a new design is required for a negative value of this parameter.

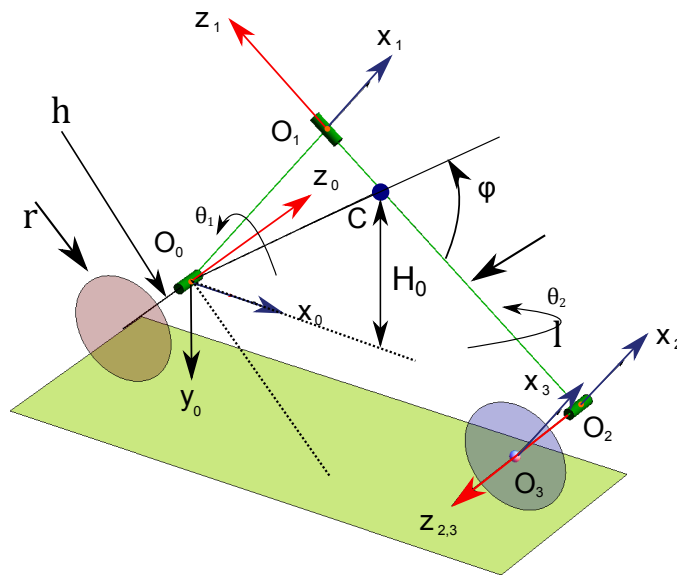


Figure 14: The simplified robotic model of the swivel car used to determine the DH parameters of the proposed mobile base.

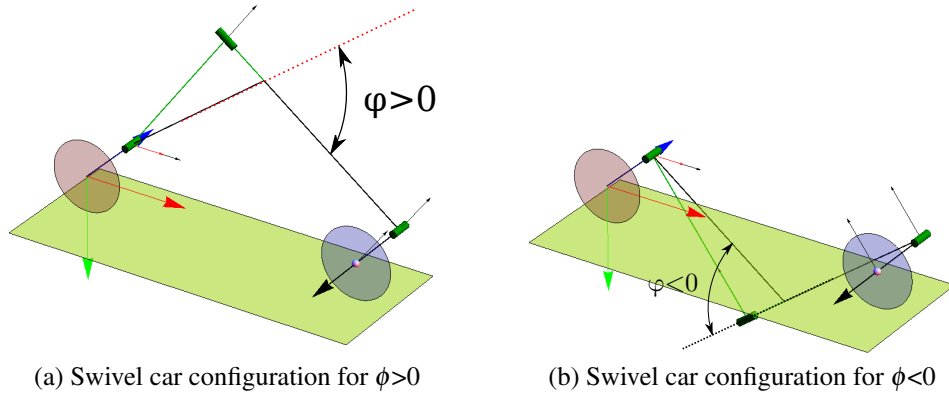


Figure 15: The change in the swivel car configuration for a position ϕ , (a), and a negative ϕ , (b).

1. DH Parameters and End-Effector Position

The swivel car can be modeled as a robotic link with two revolute joints placed at O_0 and O_1 as shown in Fig. 14 and 16. These two joints rotate about the z_0 and z_1 axis respectively as depicted in Fig. 16. Starting from the fixed origin, O_0 , we derive the DH (Denavite-Hartenberg)[15] parameters shown in Table 1. These parameters are used to establish a relationship between the initial O_0 frame and the position of the end actuator frame, O_3 . Consequently, we can represent the position of O_3 and the orientation of its axes in according to the ground frame, O_0 and its respective axes, (x_0, y_0, z_0) . The position of O_3 along with the orientation of its axes are written in terms of the design parameters (l, r, h, ϕ) and the two variable angles, θ_1 and θ_2 . Where, θ_1 is the lift angle, θ_2 is the swivel angle, h is the wheel shaft length, r is radius of the wheels, and l is the length of each ‘‘T’’ column as illustrated in Fig. 16.

Table 1: DH parameters for the first design

Joint	θ	d	a	α
1	$\theta_1 + \frac{\phi}{2} - \frac{\pi}{2}$	0	$l \sin \phi$	$-\frac{\pi}{2}$
2	θ_2	$l + l \cos \phi$	0	$-\frac{\pi}{2}$
3	θ_3	h	0	0

Utilizing the DH parameters shown in Table 1, the position of the center of the steering wheel, O_3 and the formulation of the axis of the steering wheel, \mathbf{z}_3 , in the initial

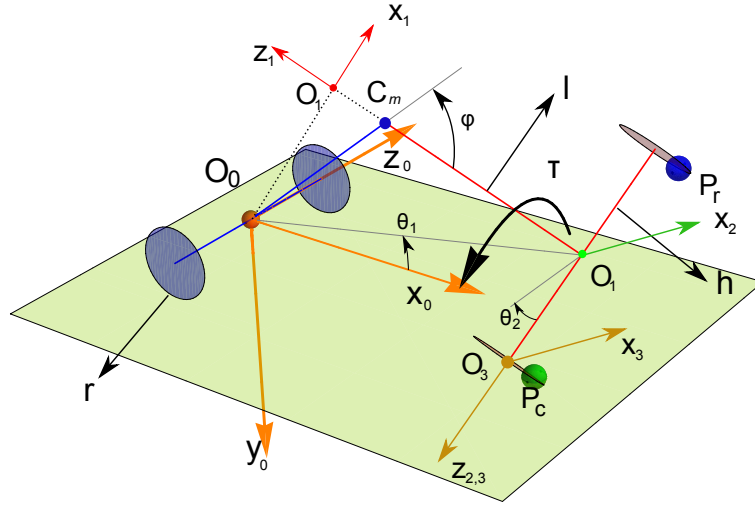


Figure 16: Skeletal representation of the swivel car along with the labeled frames and axes.

frame, O_0 can be written as,

$$O_3 = \begin{pmatrix} 2l \cos \theta_1 \cos \frac{\phi}{2} - h \sin \theta_2 \sin (\theta_1 + \frac{\phi}{2}) \\ 2l \sin \theta_1 \cos \frac{\phi}{2} + h \sin \theta_2 \cos (\theta_1 + \frac{\phi}{2}) \\ -h \cos \theta_2 \end{pmatrix}, \quad (1)$$

and,

$$\mathbf{z}_3 = \begin{pmatrix} -\sin \theta_2 \sin (\theta_1 + \frac{\phi}{2}) \\ \sin \theta_1 \cos \frac{\phi}{2} \\ -\cos \theta_2 \end{pmatrix}. \quad (2)$$

The terms (1) and (2) are of particular importance to the upcoming analysis as they represent the position of the center of the steering wheel in ground plane, and the orientation of the steering wheel in the ground frame respectively. These terms will be used to determine the motion of the steering wheel in the XZ plane and the steering capabilities of the proposed mobile base.

2. Lift Constraint

For the robot above to behave similarly to a regular mobile platform, the steering wheel must always remain in contact with the ground. To achieve this, we determine a relationship between the swivel angle, θ_2 , and the lift angle, θ_1 , such that the steering wheel, C_w , does not penetrate the ground. This relationship is determined by finding the formulation of the angle γ , shown in Fig. 17 in terms of θ_1 and then in terms of θ_2 . These two formulations are then equated to each other to determine the relationship between θ_2 and θ_1 to keep the steering wheel in contact with the ground. As

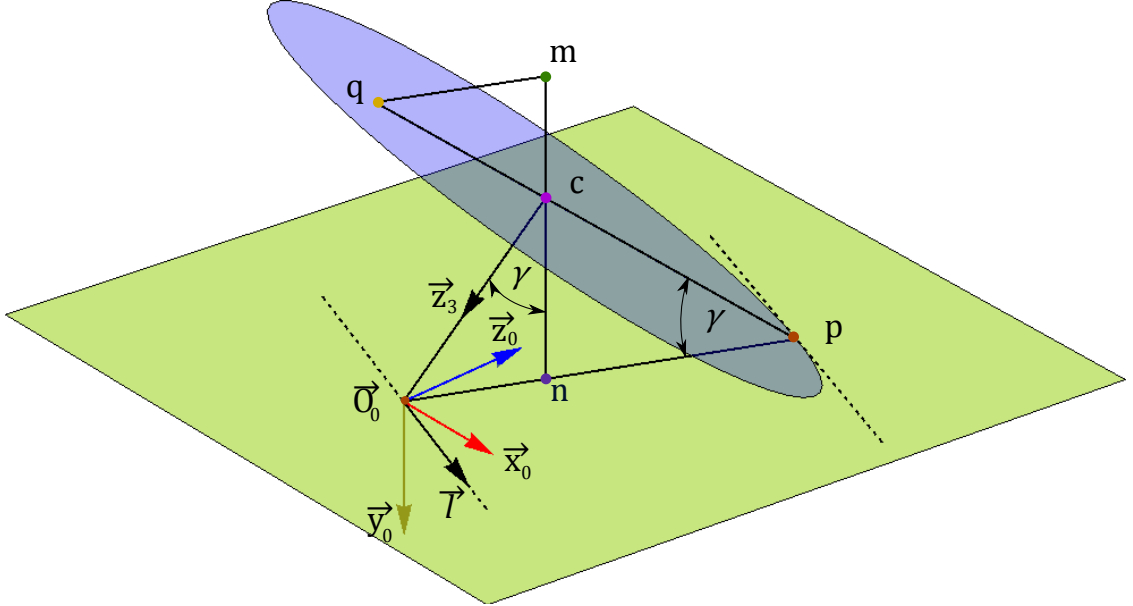


Figure 17: The steering wheel configuration and the direction of its steering axis with respect to the O_0 frame.

shown in Fig. 17, the vector z_3 makes an angle γ with the vertical line mn . The cosine of γ can be calculated by using the definition of the dot product. The dot product of \mathbf{j} and \mathbf{z}_3 is,

$$\mathbf{j} \cdot \mathbf{z}_3 = \left\| \begin{pmatrix} 0 & 1 & 0 \end{pmatrix} \right\| \cdot \|\mathbf{z}_3\| \cos \gamma \quad (3)$$

Since both \mathbf{j} and \mathbf{z}_3 are unit vectors (3) becomes,

$$\cos \gamma = \cos \left(\theta_1 + \frac{\phi}{2} \right) \sin \theta_2. \quad (4)$$

Now we proceed to determine a relationship between the height of the steering wheel center and γ . With γ known, we can then solve for the new height of the center of the front wheel which is represented by vector Cn shown in Fig. 17. Considering triangle Cpn (shown in Fig. 17), we have

$$\sin \gamma = \frac{Cn}{Cp} \Leftrightarrow \sqrt{1 - \cos^2 \gamma} = \frac{Cn}{r} \quad (5)$$

Using (5) we solve for the change in height of the wheel center from its initial location, Cm .

$$Cm = mn - Cn = r - r\sqrt{1 - \cos^2 \gamma} \quad (6)$$

Substituting the values of $\cos \gamma$ obtained in (4) into (6), and then equating (6) to the second element of the location of the end effector shown in (1), we get the relationship previously mentioned at the beginning of this part.

$$r - r\sqrt{1 - \cos^2(\theta_1 + \frac{\phi}{2}) \sin^2 \theta_2} = 2l \sin \theta_1 \cos \frac{\phi}{2} + h \sin \theta_2 \cos(\theta_1 + \frac{\phi}{2}). \quad (7)$$

The above equation can be solved analytically to determine the change in θ_1 , as a function of the swivel angle, θ_2 . This solution will be referred to as the lift constraint throughout the remainder of this thesis. Fig. 18 (a) shows the variation of the lift angle, θ_1 , versus the swivel angle θ_2 for the positive values of ϕ , whereas Fig. 18 (b) illustrates the value of θ_1 versus the variation in θ_2 for the negative values of ϕ . When θ_2 is actuated in either the clockwise or counter-clockwise direction, the car rotates about its back wheel axis, z_0 . Consequently, the lift constraint produces a symmetric function when θ_2 varies from $-\frac{\pi}{2}$ to $\frac{\pi}{2}$. Note that when ϕ is negative, the relationship between θ_1 and θ_2 does not vary greatly for different values of ϕ . Furthermore, when ϕ is positive the steering wheel moves towards the back wheel axis z_0 , whereas the opposite occurs for a negative ϕ as shown in Fig. 19a and 19b respectively

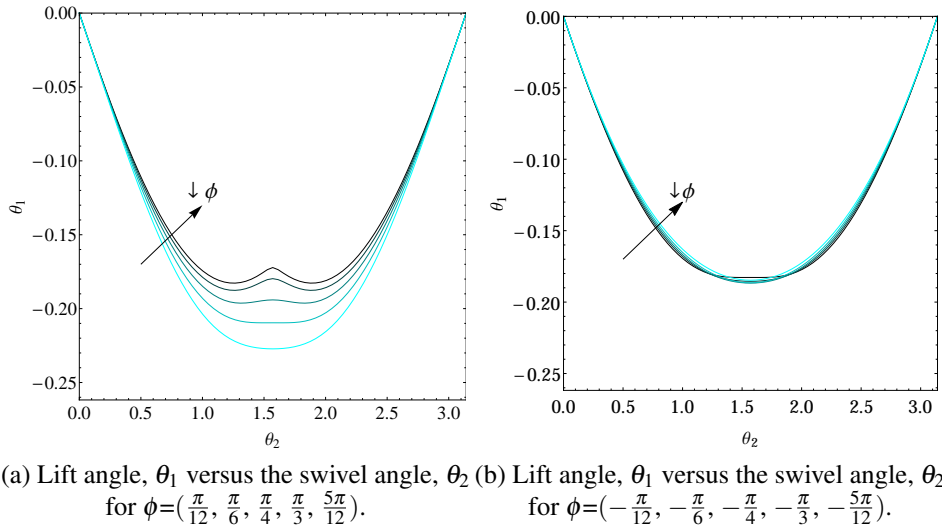


Figure 18: The effects of varying ϕ on the lift constraint. The figure to the left depicts this variation for positive values of ϕ , whereas the figure on the right depicts this relationship for a negative ϕ

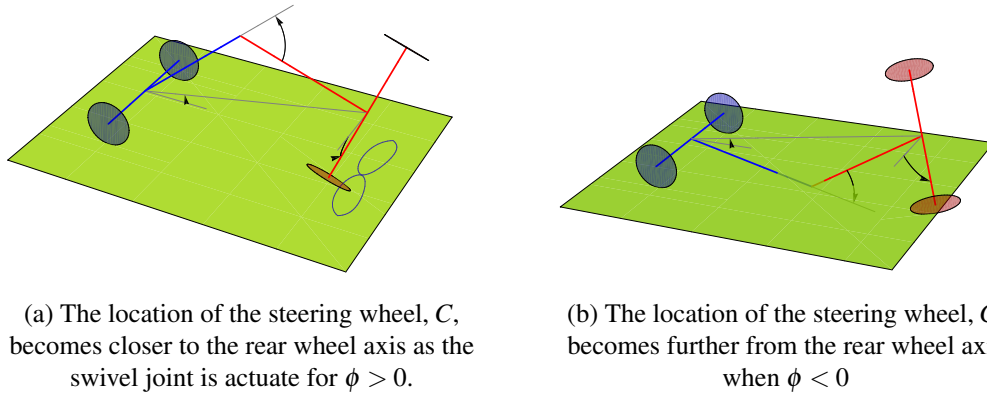


Figure 19: The effects of changing the sign of ϕ on the motion of the front steering wheel.

3. Point of Contact Analysis

Now we solve for the point of contact, p , of the steering wheel, C_w , with respect to the XZ ground plane. Using the kinematics previously developed, one can solve for the location of the point p starting from the location of the steering wheel, C_w , and the axis of rotation, z_3 , which were determined in (1) and (2). By referring to Fig. 17, we start by translating along the y_0 axis by a distance of $r \sin \gamma$, and then along the vector \mathbf{Op} by a distance of $r \cos \gamma$. The vector \mathbf{Op} is calculated by projecting the unit vector, \mathbf{z}_3 , on the XZ plane. A unit vector along \mathbf{Op} can be calculated by taking the cross product of

the vectors \mathbf{j} and \mathbf{v} , and then rotating this vector about the y_0 axis by an angle of $-\frac{\pi}{2}$. Finally, the resulting vector is normalized. Consequently, the position of the contact point can be written as,

$$p = C + r \sin \gamma \mathbf{j} + r \cos \gamma \frac{\mathbf{Op}}{\|\mathbf{Op}\|}, \quad (8)$$

where,

$$\mathbf{Op} = \mathbf{j} \times \mathbf{z}_3. \quad (9)$$

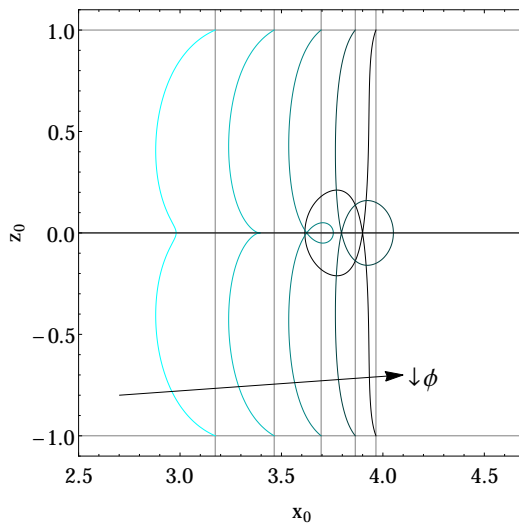
Substituting (9) into (8) results in the following formulation for p ,

$$p = C + r \sin \gamma \mathbf{j} + r \cos \gamma R_{\mathbf{j}, -\frac{\pi}{2}} \frac{\mathbf{j} \times \mathbf{z}_3}{\|\mathbf{j} \times \mathbf{z}_3\|}, \quad (10)$$

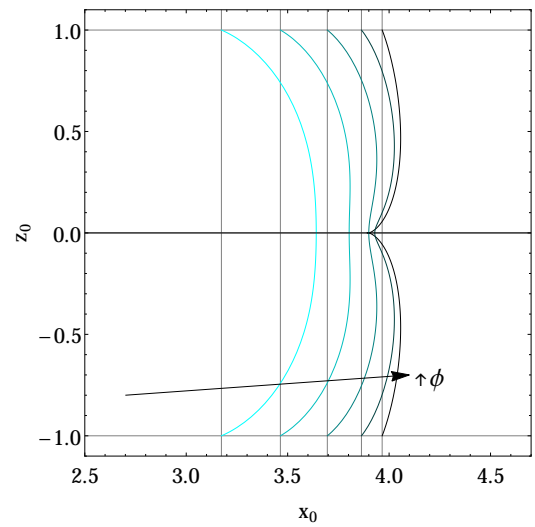
where $R_{\mathbf{j}, -\frac{\pi}{2}}$ is a rotation about the y_0 axis by an angle of $\frac{\pi}{2}$ in the clock-wise direction.

Substituting (5) and (6) into (10) allows us to solve for the location of p for different values of θ_2 . This equation is solved to obtain the graphs shown in Fig. 20a and 20b.

These two graphs illustrate path followed by the point of contact, p , for several values of the parameter ϕ with respect to the O_0 frame located at the back of the swivel car. The path followed by p is further illustrated by the multiple frames shown in Fig. 20. The swivel angle, θ_2 , was varied from 0 to $\frac{\pi}{2}$ for $\phi = \frac{5\pi}{12}$.



(a) Path followed by the point of contact in the XZ plane for $\phi = (\frac{\pi}{12}, \frac{\pi}{6}, \frac{\pi}{4}, \frac{\pi}{3}, \frac{5\pi}{12})$



(b) Path followed by the point of contact in the XZ plane for $\phi = (-\frac{\pi}{12}, -\frac{\pi}{6}, -\frac{\pi}{4}, -\frac{\pi}{3}, -\frac{5\pi}{12})$

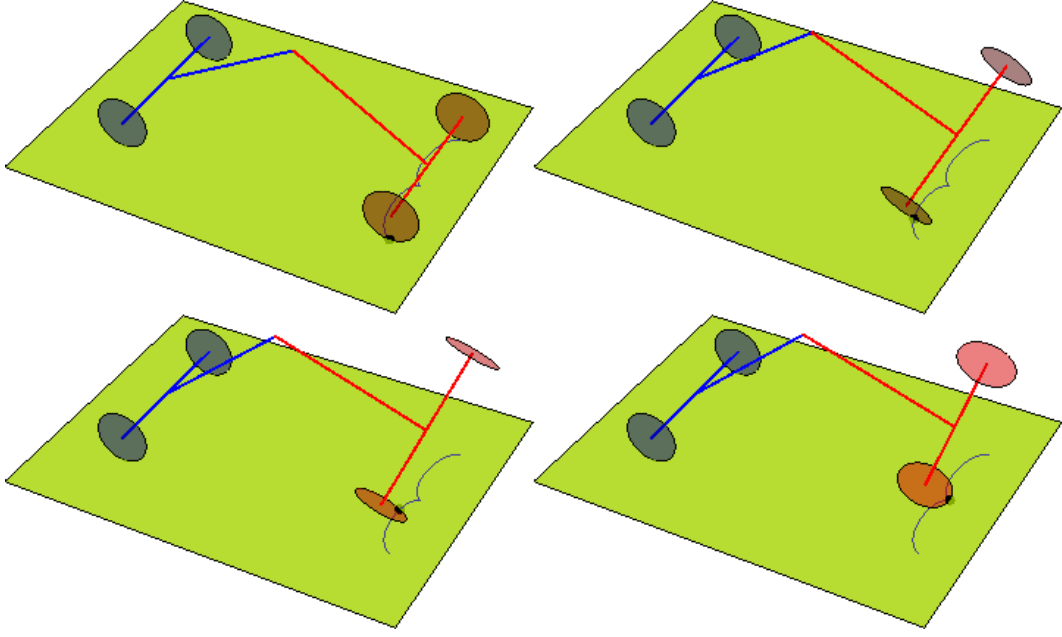


Figure 20: Four frames illustrating the path of p in the XZ plane as θ_2 varies from 0 to $\frac{\pi}{2}$ for $l=20$ cm, $h=10$ cm, $\phi = \frac{\pi}{6}$ and $r=0.33$ cm

Examining Fig. 20a and 20, we notice that for the positive values of ϕ the path followed by p changes drastically from one value of ϕ to another. On the other hand, for negative values of ϕ the path followed by p does not greatly vary when the parameter ϕ is varied.

4. Steering Capabilities

In this part of Section II, we study the steering capabilities of the mobile platform using the model kinematics derived above. In short, we aim to derive a relationship between the swivel angle, θ_2 , and the steering angle, θ . Similar to a bicycle or a car, the steering angle of the swivel car can be determined by calculating the angle between the projections of the front and back wheel axis on the ground plane, XZ . The point at which these two projections intersect forms the center of instantaneous rotation. In our case, it is sufficient to determine the angle between the vector \mathbf{i} and the vector \mathbf{I} , both of which are shown in Fig. 17. The vector \mathbf{I} can be obtained by calculating the cross

product of \mathbf{j} and \mathbf{z}_3 , where \mathbf{j} is the unit vector along the y_0 axis shown in Fig. 16.

$$\mathbf{l} = \mathbf{z}_3 \times \mathbf{j} = \begin{pmatrix} \cos \theta_2 \\ 0 \\ -\sin \theta_2 \sin(\theta_1 + \frac{\phi}{2}) \end{pmatrix}. \quad (11)$$

We now compute the cosine of the steering angle, θ , by calculating the dot product of the vectors \mathbf{i} and \mathbf{v} ,

$$\mathbf{i} \cdot \mathbf{v} = \|\mathbf{i}\| \|\mathbf{l}\| \cos \theta. \quad (12)$$

After substituting the values of \mathbf{l} and \mathbf{i} into (12), the cosine of the steering angle can be written as,

$$\cos \theta = \frac{\cos \theta_2}{\sqrt{\cos^2 \theta_2 + \sin^2 \theta_2 \sin^2(\theta_1 + \frac{\phi}{2})}}. \quad (13)$$

Plugging in the solution of (6) into (13) allows us to solve for the value of the steering angle in terms of the swivel angle, θ_2 . Fig. 21a and 21b show the variation of the steering angle versus the change in θ_2 for different values of ϕ .

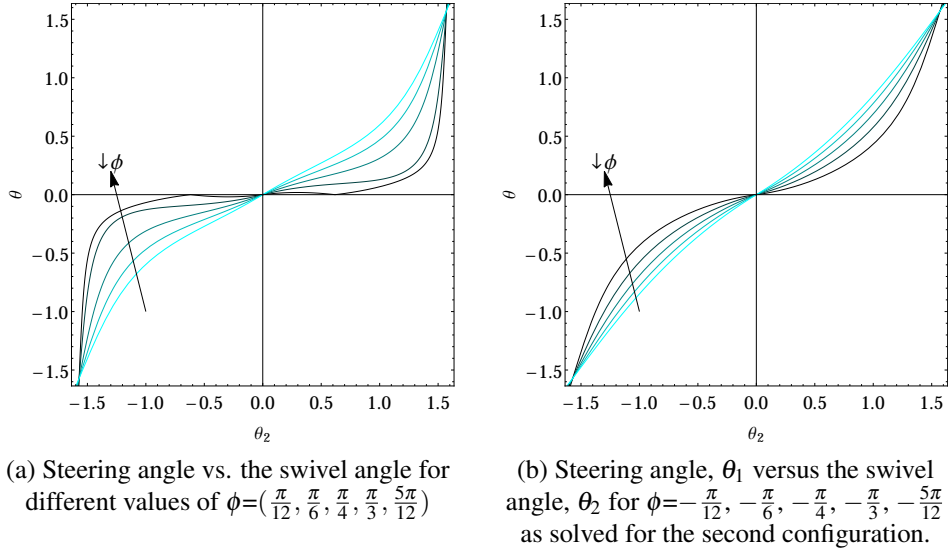


Figure 21: Steering angle versus the change in the twist angle, θ_2 , for different values of the design parameter ϕ

Comparing Fig. 21a and 21b, we notice that the swivel car passes better

steering capabilities for a negative value of ϕ rather than a positive one. For example the steering angles for $\phi = \frac{\pi}{3}$ and $\phi = -\frac{\pi}{3}$ are respectively 0.5 rad. and 0.75 rad. From the figures, we can further deduce the effects of the parameter ϕ on the steering angle. When ϕ is negative, the steering angle does not significantly vary from one configuration to the other. However, for positive values of ϕ , we notice a significant variation from one value to the next.

It should be noted when the swivel joint is actuated in the clockwise direction, the mobile base steers in the clockwise direction for a positive value of ϕ . On the other hand, the swivel car steers in the counter-clockwise direction for a negative value ϕ . This difference in steering capabilities is further illustrated in Fig. 22a and 22b. Fig. 22a depicts the steering angle and point of steering for $\phi > 0$. Fig. 22b illustrates these terms for $\phi < 0$. As can be seen in Fig. 21, the proposed mobile base possesses excellent

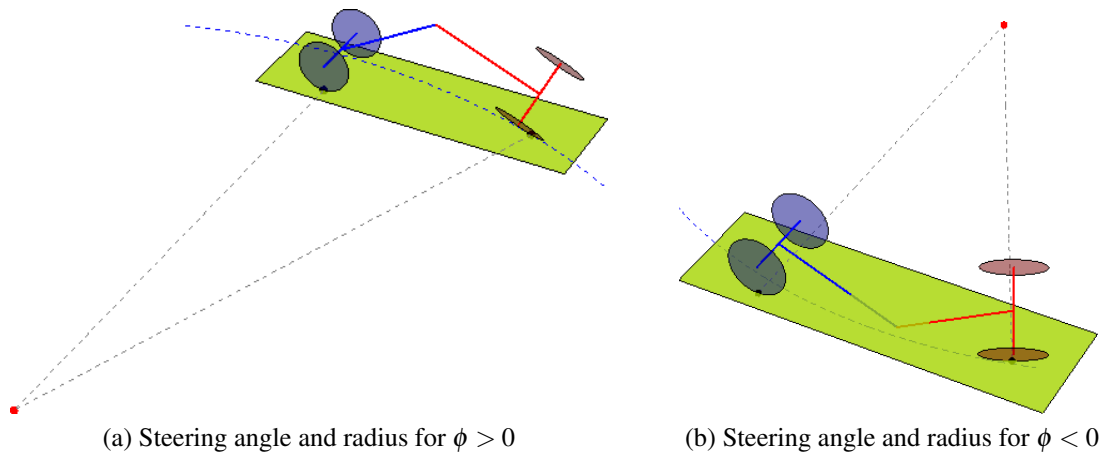


Figure 22: Change in the steering kinematics of the mobile base for a positive(left) and negative(right) value of ϕ

steering capabilities. It is capable of achieving a steering angle of $\frac{\pi}{2}$ meaning it can rotate about its own axis without changing in position on the ground plane.

5. Step Climbing Kinematics of the swivel car

In this part of Section II, we analyze the step climbing capabilities of the swivel car by extending the kinematic analysis conducted in B.. For simplification, we assume the swivel car can climb steps by lifting the base of one of its front wheels above a desired height. As such, to determine the maximum scalable step of the swivel car it is sufficient to determine the height of the lowest point on the lifted front wheel, P_L . We first start by finding the location of any point, P_r , that lies on the circumference of the lifted wheel. This is done by implementing the following four transformations about the O_3 frame shown in Fig. 16,

1. Rotation about the z_3 axis by an angle of $\frac{\pi-\phi}{2}$ so that the new x-axis is parallel to the y_0 axis shown in Fig. 16.
2. Translation about the z_3 axis by a distance of $2h$.
3. Translation about the new z-axis by a distance r .

A sketch detailing the location of an arbitrary point, P_r , and the lowest point, P_L , with respect to the lifted wheel is shown in Fig. 23. The angle θ_3 refers to the angular position of an arbitrary point lying on the circumference of the lifted wheel, and the angle θ_{3sol} is the angle at which P_r is closest to the ground plane, XZ i.e. it is the angle at which P_L is located with respect to the x-axis of the lifted wheel. Solving for the transformations above one can obtain the height, y_r of the any arbitrary, P_r , lying on the circumference of the lifted wheel, where

$$y_r = (l + l \cos \phi + r \cos(\frac{1}{2}(\phi - 2\theta_3))) \sin(\theta_1 - \frac{\phi}{2}) + \cos(\theta_1 - \frac{\phi}{2})(-h \sin \theta_2 + l \sin \phi + r \cos \theta_2 \sin(\frac{1}{2}(\phi - 2\theta_3))). \quad (14)$$

Fig. 24 shows the variation in height of P_r with respect to the change in θ_3 for different values of θ_2 . Upon close examination, we notice that the lowest position for P_r

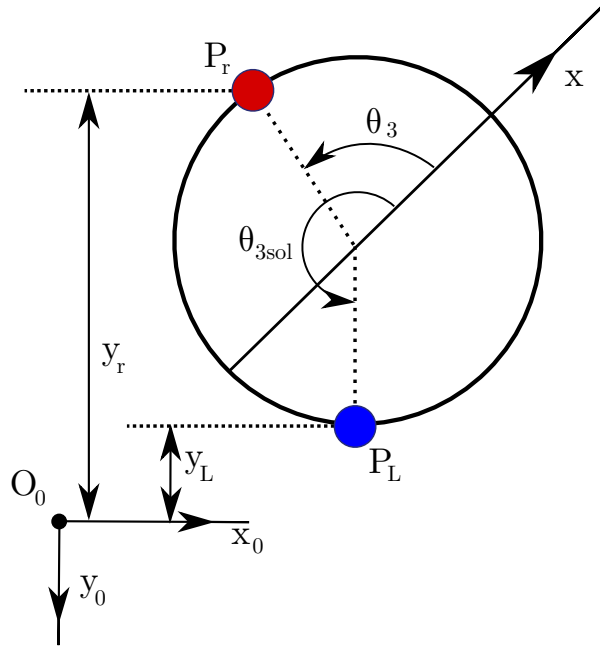


Figure 23: Sketch of the wheel showing the location of P_r and P_L with respect to an inertial frame O_0

occurs when the derivative of (14) with respect to θ_3 is equal to zero as shown below,

$$\frac{\partial y_p}{\partial \theta_3} = 0. \quad (15)$$

Solving (15) results in the following formulation of θ_3 ,

$$\theta_{3sol} = -\arccos\left(\frac{\sin \theta_1 + \sin(\theta_1 - \phi)}{\sqrt{\cos^2 \theta_2 \cos^2(\theta_1 + \frac{\phi}{2}) + \sin^2(\theta_1 + \frac{\phi}{2})} + \frac{2 \cos \theta_2 \cos(\theta_1 - \frac{\phi}{2}) \sin \frac{\phi}{2}}{\sqrt{\cos^2 \theta_2 \cos^2(\theta_1 + \frac{\phi}{2}) + \sin^2(\theta_1 + \frac{\phi}{2})}}}\right) \quad (16)$$

Consequently, we determine the lowest possible location for p_r by substituting θ_{3sol} determined in (16) into (14). Fig. 25 shows the height of the lowest point on the lifted wheel with respect to the swivel angle for the dimensions shown in Table 2. Note that, the chosen dimensions are similar in height, length, and mass distribution to the car-like robot proposed and tested in [2]. Furthermore, Fig. 26 and 27 show the height of the lowest point on the lifted wheel for different values of ϕ and h respectively. Finally, we

Table 2: Simulation parameters

Parameter	Value	Label
m_s	21 Kg	Mass of Robot
I_s	0.84 kgm^2	Inertia of Robot
l	25 cm	Length of "T" Column
h	15 cm	Wheel Shaft Length
ϕ	$\frac{\pi}{3}$	Angle Between "T" Columns
r	7.5 m	Wheel Radius
K_p	19	Proportional Gain
K_d	5.5	Derivative Gain
K_I	11.45	Integral Gain

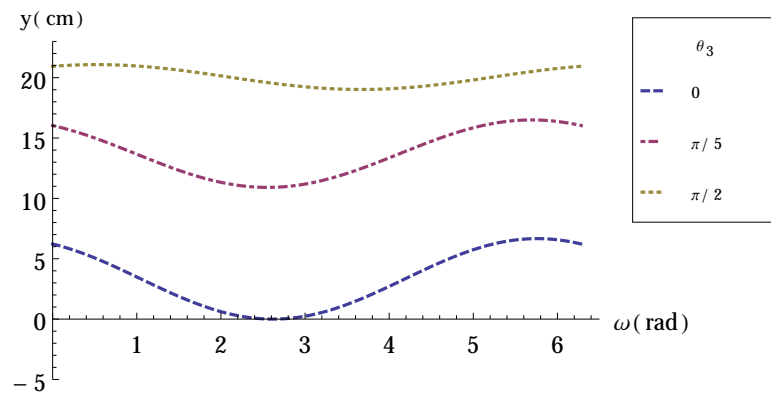


Figure 24: Height variation of the random point P_r about the circumference of the lifted wheel for different values of θ_2

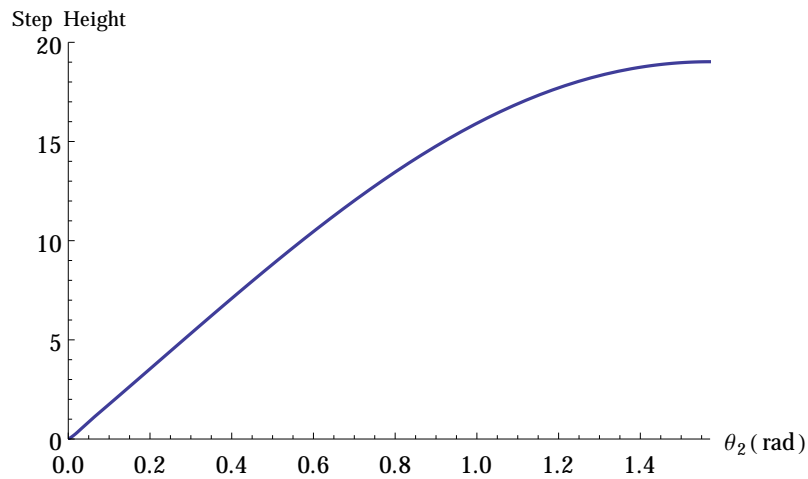


Figure 25: The height of the lowest point, P_l , as a function of the swivel angle, θ_2

study the effects of changing the parameters l and r on the robots climbing capabilities.

Fig. 28 and 29 depict the maximum scalable step for different values of l and r . Upon

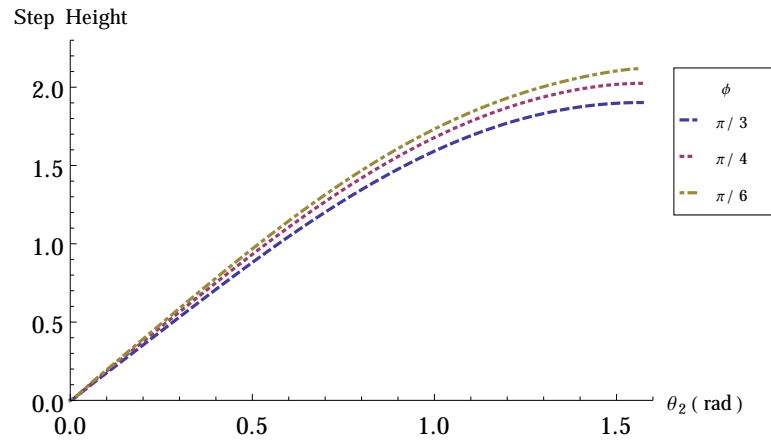


Figure 26: Change of step climbing capabilities as ϕ varies

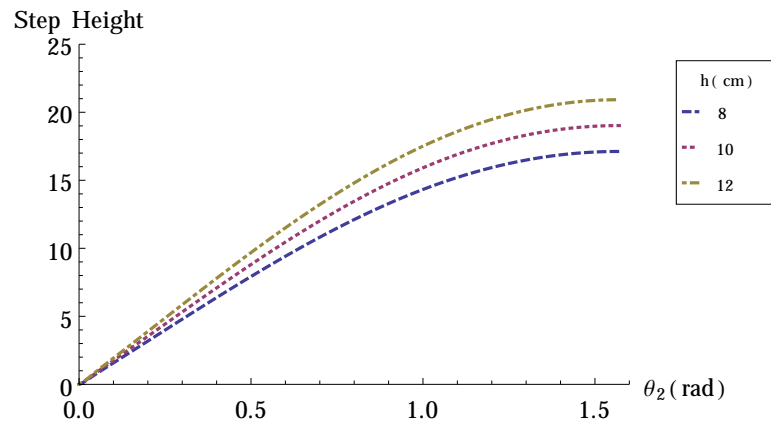


Figure 27: The effect of changing the wheel shaft length h , on the maximum scalable step

examining these figures, we notice that there is no change in the robot's climbing capabilities when these two parameters are varied.

According to Fig. 25, the swivel car is capable of climbing obstacles equal in height to the wheel diameter. However, upon further investigation, we notice the step climbing capabilities are independent of the wheel diameter, rather they are dependent on the the wheel shaft length, h , and the angle ϕ , both of which are robot geometric parameters. Figs. 26 and 27 show the variation of the swivel car's step climbing capabilities with the change of ϕ and h , respectively. However, as we will see in the next part, an increase in h is followed by a proportional increase in the required torque to lift

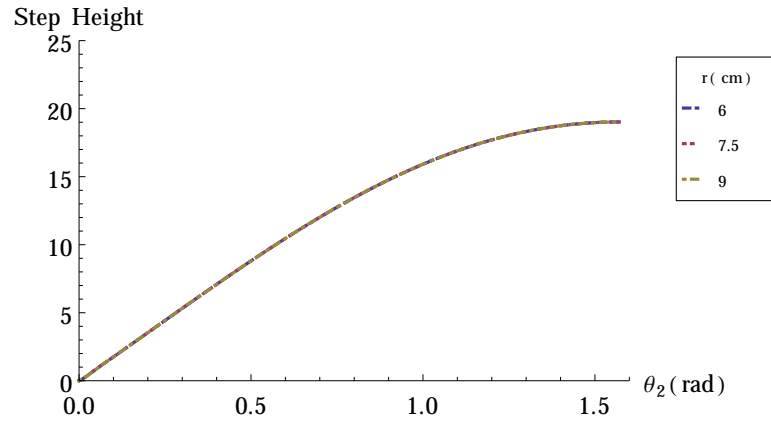


Figure 28: The effect of changing the length of “T” column, l on the maximum scalable step.

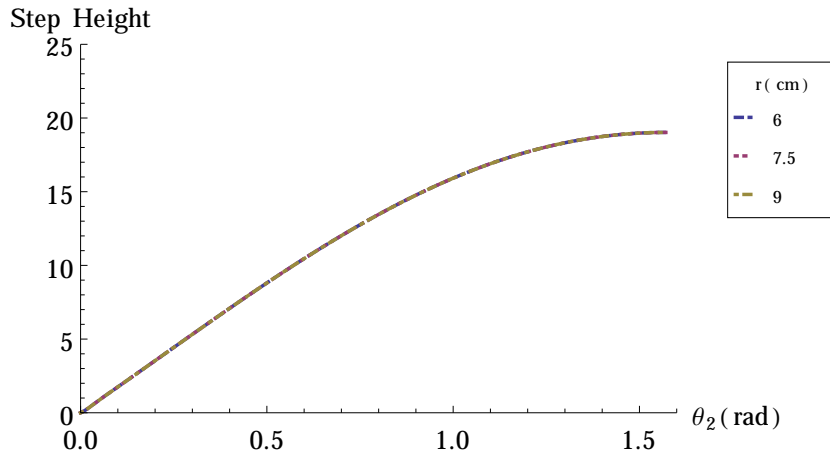


Figure 29: The effect of changing the wheel radius, r , on the maximum scalable step.

the wheel. This limits the maximum shaft length and step climbing capabilities.

C. Dynamics of the Steering Mechanism

In this part of Section II, we start by analyzing the dynamics of actuating the swivel joint to achieve steering. Through this analysis, we determine the torque requirements to achieve steering as well as the energy expended during steering. Next, we extend this dynamics analysis to calculate the peak torque requirement for climbing a step along with the total expended energy during step climbing.

1. Dynamic Analysis of the Steering Mechanism

Now, we create a simplified dynamic representation of the swivel car to model the step climbing energy costs by modeling the steering mechanism. Through these simulations, we determine the total expended energy while climbing a step, and the peak torque requirement at the swivel joint for both steering and step climbing. The results of this simulation are compared to examples from literature to assess the performance of the swivel car as a step climbing robot. To simplify the system, we first assume the entire mass of the car is concentrated at the point-mass, C_m (shown in Fig. 16). Furthermore, during the actuation of the swivel joint, we assume this point mass rotates about the fixed axis z_0 with an angle θ_1 as shown in Fig. 16. To model the system, we use the Lagrange-Euler formulation [17], where the system's kinetic energy, T_s , and potential energy, V_s , are respectively given by

$$T_s = \frac{I_s \dot{\theta}_1^2}{2}, \quad (17)$$

$$V_s = m_s g \Delta H. \quad (18)$$

Here, m_s is the mass of the car, I_s is the inertia of the swivel car about the rear wheel axis, z_0 , and ΔH is the change in height of the center of mass. Thus, the Lagrangian is

$$L_s = T_s - V_s. \quad (19)$$

Substituting (17) and (18) into (19) yields,

$$L_s = \frac{I_s \dot{\theta}_1^2}{2} - m_s g \Delta H, \quad (20)$$

with,

$$\Delta H = H_o - H_i, \quad (21)$$

where H_o is the initial height of point C_m , and H_i is the current height of C_m which varies with θ_1 . H_o , can be determined using the following equation,

$$H_o = l \sin\left(\frac{\pi}{2} - \frac{\phi}{2}\right). \quad (22)$$

The height of C_m versus the swivel angle, θ_2 , can be obtained by performing a translation along the z-axis of O_1 shown in Fig. 16 by $l \cos \phi$, and can be written as,

$$H_i = l \cos \phi \sin\left(\theta_1 + \frac{\phi}{2}\right) - l \cos\left(\theta_1 + \frac{\phi}{2}\right) \sin \phi. \quad (23)$$

Substituting (23) and (22) into (20) results in the following formulation for L_s

$$L_s = \frac{I_s \dot{\theta}_1^2}{2} - m_s g \left(l \sin\left(\frac{\pi}{2} - \frac{\phi}{2}\right) - \cos \phi \sin\left(\theta_1 + \frac{\phi}{2}\right) - l \cos\left(\theta_1 + \frac{\phi}{2}\right) \sin \phi \right). \quad (24)$$

As shown in [14], the angle θ_1 can be written in terms of the swivel angle θ_2 , this means (24) can also be written as a function of the controlled variable θ_2 . Finally, using the Euler-Lagrange formulation, we compute the equations of motion to get

$$\frac{\partial}{\partial t} \frac{\partial L_s}{\partial \dot{\theta}_2} - \frac{\partial L_s}{\partial \theta_2} = \tau_s. \quad (25)$$

An external torque, τ , is used to control the angular position of the swivel joint by implementing a PID controller of the form,

$$\tau_s = K_p(\theta_{2d} - \theta_2) + K_D \dot{\theta}_2 + K_I \int_0^t (\theta_{2d} - \theta_2) dt, \quad (26)$$

where θ_{2d} is the desired value of the swivel angle, and (K_p, K_I, K_D) are the PID gains used for angular position control of the swivel joint.

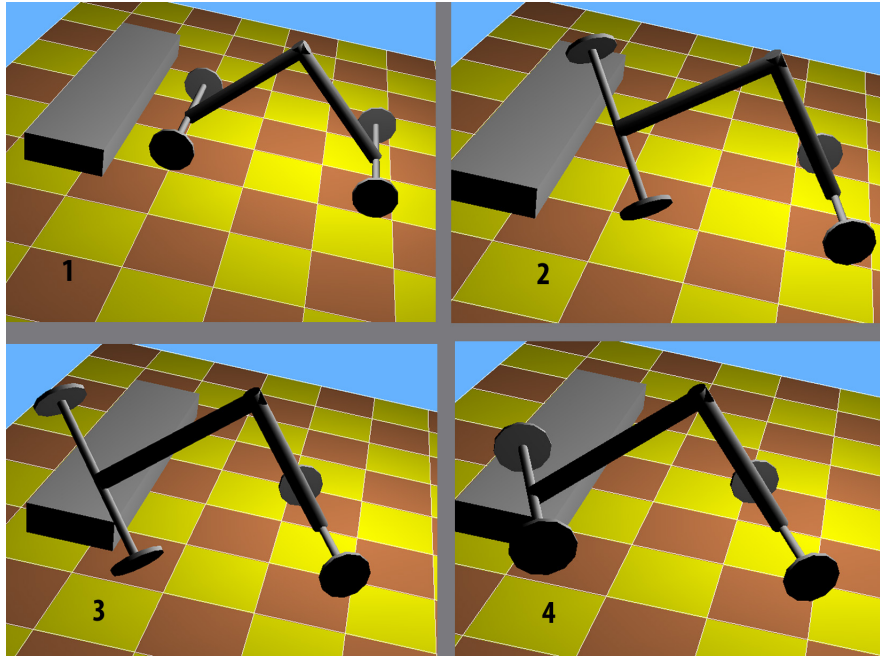


Figure 30: The swivel car climbing an obstacle by actuating the swivel joint, which also acts as its steering mechanism

2. *Cost of Climbing a Step*

The step climbing process can be divided into three parts. In the first part the vehicle lifts one of its front wheels above the step, and in the second part the robot moves forwards until the base of its lifted wheel is just above the step. Finally, the swivel car lifts the rest of its body above the step as illustrated in Fig. 30. The model derived in (25) was solved in Mathematica for the dimensions shown in Table 2. For verification, a model of the swivel car was also created in Dymola using the Multibody Library [18]. For comparison purposes with the results of [2], we will simulate the swivel car as it climbs a 12mm step. This is done by actuating the swivel angle to 0.12 rad (6.6°). At this angle, the base of the lifted wheel lies just above the step. The results of these simulations are shown in Fig. 31 which shows the torque applied at the swivel joint for lifting one wheel (blue), and for lifting the rest of the car (red), and represents the energy consumption versus time for lifting the wheel (blue), and for lifting the rest of the car (red). Examining the results of the simulation in Fig. 31, the peak torque applied at the swivel joint is 8 Nm. which is 20 percent greater than the results present in literature for

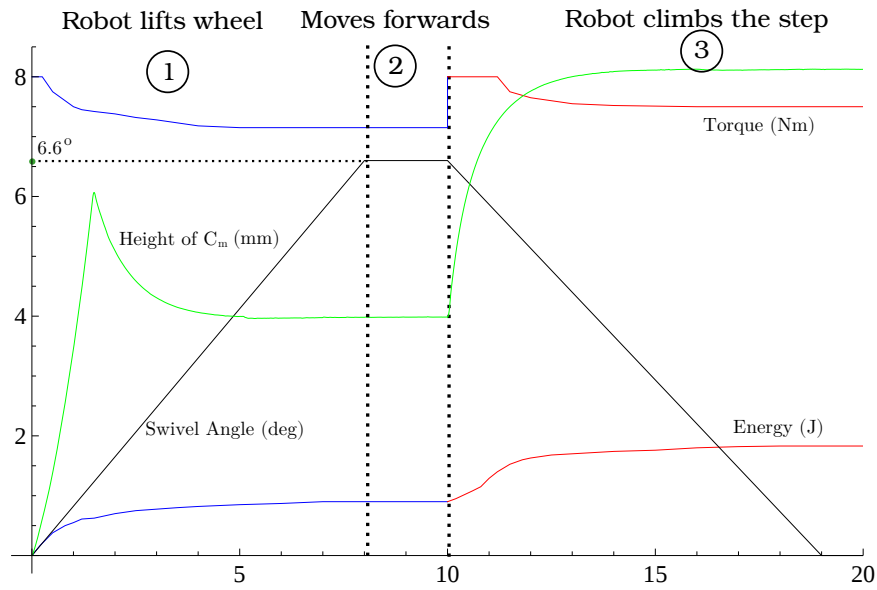


Figure 31: A graph showing the expended energy during a step climbing process, along with the peak torque as the swivel angle changes

a car-like robot of the same build [2], and the expended energy is 3 J versus 3.2 J for the car-like robot.

3. Dependency of Peak Torque on h

We now investigate the effects of varying the parameter h on the peak torque required at the twist joint. The study was conducted for multiple values of this parameter and can be seen in Fig. 32. The figure depicts a linear relationship between the increase in the wheel shaft length, h , and the peak torque required at the twist joint. The conducted analysis serves to verify our previous statements concerning the effects of increasing the length of the wheel shaft on the dynamics of the proposed mobile base.

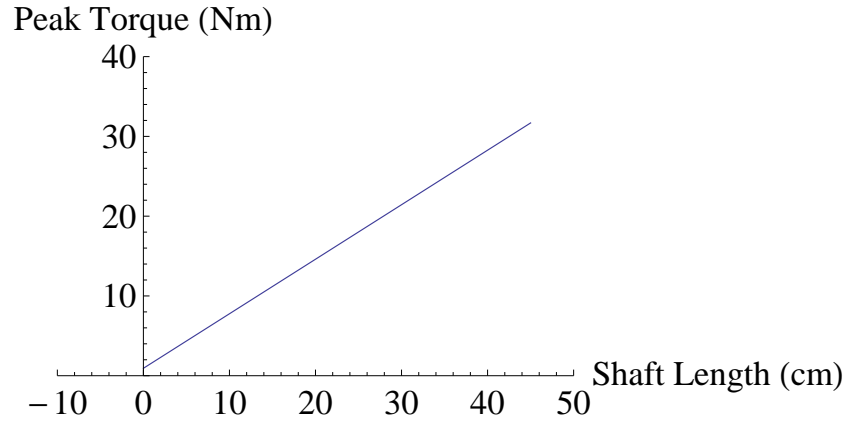


Figure 32: A plot depicting the change peak torque at the swivel joint to climb a step versus the increase in h .

D. Platform Model with Nonholonomic Constraints

In this part of Section II, we investigate the dynamic effects of actuating the swivel joint on the position and orientation of the swivel car. In previous sections, the model of the swivel car was constrained such that no rotation occurs about the y_0 axis, and no change of position occurs in the XZ plane. However, multibody simulations conducted in Dymola indicate that these two assumptions are not correct. In fact, as the steering of the platform is actuated, our simulations indicate that the rear wheel axle does not remain stationary.

1. Nonholonomic Constraints

Before we analyze the platform dynamics of the swivel car, we briefly explain the theory behind nonholonomic constraints. The motion of a regular wheel, such as the one shown in Fig. 33, is constrained such that:

1. The wheel does not slip in the lateral direction along C_0 (no skidding).
2. The wheel does not slip along V_0 while revolving about its axis (no slipping), meaning the wheel's linear velocity is equal to its angular velocity multiplied by the radius of the wheel.

These two constraints are referred to as nonholonomic constraints, and are at the basis of the modeling wheeled mobile platforms.

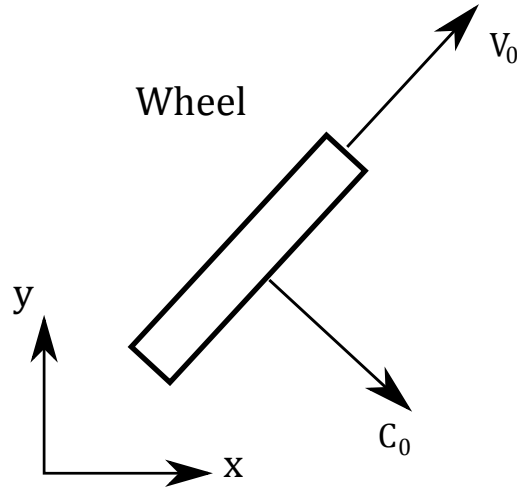


Figure 33: A single wheel as seen from above with its nonholonomic constraints.

No Slip Condition The wheel does not slip along C_0 , consequently the projection of the wheel's velocity in this direction is equal to zero. Mathematically, this relationship can be written as

$$C_0 = r_0 v_0, \quad (27)$$

where r_0 is the unit vector along C_0 , and v_0 is the linear velocity of the wheel. To impose this relationship, we assume the wheel is capable of exerting a reaction force along C_0 to counteract any external force. This force, F_0 , prevents the wheel from moving in the lateral direction along C_0 by canceling out any external forces applied along C_0 . To compensate for a wide variety of forces, F_0 is written in terms of a Lagrange multiplier, λ_0 . Therefore, the nonholonomic reaction force for a single wheel is,

$$F_0 = \lambda_0 r_0. \quad (28)$$

2. Platform Model

For a better understanding of the car's steering dynamics, we create another simplified two dimensional model of the swivel car to capture the effect of steering on the actual position and orientation of the platform. We do this by projecting the motion of the robot onto the XZ plane. From the kinematic analysis, while analyzing the steering capability of the swivel steering car, we noted the motion of the contact point between the steering wheel and the ground. In fact, since the rear wheel axis was stationary, it was evident that the motion of the contact point violates the sideways skidding constraint of the steering wheel. In this section, we enforce the non-skidding constraint on all the wheels including the steering wheel. Thus, we allow the rear axle to move and change orientation accordingly. In other words all nonholonomic constraints [19] are always respected. In particular this means the wheels of the robot do not skid in the lateral direction along C_1 or C_2 as illustrated in Fig. 34. The simplified model can reproduce the effects of actuating the swivel joint on the position and orientation of the platform by simulating the motion of the steering wheel. This is done by replacing the out-of-plane swivel joint by three planar joints in the simplified model. Two prismatic joints, u and v , are used to trace the path followed by the wheel in the XZ plane, whereas a rotational joint, α , acts as the steering angle and rotates about the normal axis to the XZ plane. Finally, we assume the majority of the robot's mass is concentrated in p_1 , while the remainder of the mass is equally distributed about the four wheels. Fig. 34 shows a free body diagram of the simplified model, along with the placement of masses and the location of the actuators. The system's equations of motion are determined using the Euler-Lagrange formulation. The configuration of the simplified model comprises of six generalized coordinates, $q = \{x, z, \theta, u, v, \alpha\}$. Note that the actuated degrees of freedom, u , v , and α , are a function of the swivel angle θ_2 as dictated by the kinematic analysis. We begin with the computation of the equations of motion by first determining

the location of the centers of mass, $p = (p_a, p_b, p_1, p_c, p_d)$ with,

$$p_a = \begin{pmatrix} x \\ z \end{pmatrix}, \quad (29)$$

$$p_b = p_a + \begin{pmatrix} -2h \sin \theta \\ 2h \cos \theta \end{pmatrix}, \quad (30)$$

$$p_1 = p_a + \begin{pmatrix} l \cos \theta - h \sin \theta \\ l \sin \theta + h \cos \theta \end{pmatrix}, \quad (31)$$

$$p_d = p_1 + \begin{pmatrix} (h+v) \sin \theta + (l+u) \cos \theta \\ (l+u) \sin \theta - (h+v) \cos \theta \end{pmatrix}, \quad (32)$$

$$p_c = p_1 + \begin{pmatrix} -(h+v) \sin \theta + (l+u) \cos \theta \\ (l+u) \sin \theta + (h+v) \cos \theta \end{pmatrix}. \quad (33)$$

Taking the derivative of p with respect to time yields the velocity of these five points

$v = (v_a, v_b, v_1, v_c, v_d)$. The position of the contact point of the steering wheel in the XZ

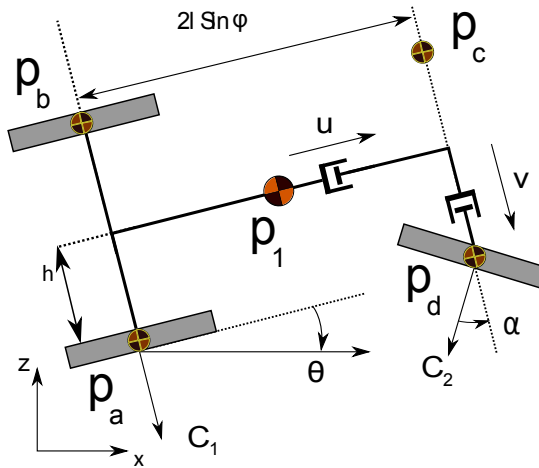


Figure 34: Simplified swivel car model with nonholonomic constraints modeled as a 2D planar mechanism

plane can be written as,

$$x_p = 2l \cos \frac{\phi}{2} + u, \quad (34)$$

$$z_p = v, \quad (35)$$

where x_p and z_p are the paths followed by the point of contact as represented in a body coordinate frame attached to the middle of the rear axle. To capture the kinematics of the angular swivel steering, an inverse dynamic controller, Q [20], is applied to the generalized coordinates (u, v, α) as a function of the swivel angle θ_2 . With

$$Q = \ddot{q} + 2\zeta\omega(\dot{q}_p - \dot{q}) + \omega^2(q_p - q), \quad (36)$$

where $q_p = (0, 0, 0, u_p, v_p, \alpha_p)$ is the vector of the controlled coordinates, $\omega = (0, 0, 0, \omega_u, \omega_v, \omega_\alpha)$ and $\zeta = (0, 0, 0, \zeta_u, \zeta_v, \zeta_\alpha)$ are the respective gains and damping of the inverse dynamic controller. The Lagrangian is given by

$$L = \frac{m_w}{2}(v_a v_a^T + v_b v_b^T + v_c v_c^T + v_d v_d^T) + \frac{m_b}{2} v_1 v_1^T + I_{w1}(2\dot{\theta}^2) + \frac{I_{car}}{2} \dot{\theta}^2 + I_{w2} \alpha \dot{\alpha}^2. \quad (37)$$

To obtain the equations of motion we follow the Euler-Lagrange formulation to arrive at,

$$\frac{d}{dt} \left(\frac{\partial L}{\partial \dot{q}} \right) - \frac{\partial L}{\partial q} = Q + f_g, \quad (38)$$

where f_g is the set of forces due to the nonholonomic constraints of the wheels and can be written as,

$$f_g = F_1 \frac{\partial p_a}{\partial q} + F_2 \frac{\partial p_b}{\partial q}, \quad (39)$$

with,

$$F_1 = \begin{pmatrix} \cos(\theta - \frac{\pi}{2}) \\ \sin(\theta - \frac{\pi}{2}) \end{pmatrix} \lambda_1 + \begin{pmatrix} \cos(\theta - \frac{\pi}{2}) \\ \sin(\theta - \frac{\pi}{2}) \end{pmatrix} \lambda_2, \quad (40)$$

and,

$$F_2 = \begin{pmatrix} \cos(\theta + \alpha - \frac{\pi}{2}) \\ \sin(\theta + \alpha - \frac{\pi}{2}) \end{pmatrix} \lambda_1 + \begin{pmatrix} \cos(\theta + \alpha - \frac{\pi}{2}) \\ \sin(\theta + \alpha - \frac{\pi}{2}) \end{pmatrix} \lambda_2, \quad (41)$$

where λ_1 and λ_2 are the Lagrange multipliers. The vector of generalized coordinates, q is,

$$q = \begin{pmatrix} x \\ y \\ \phi_i \\ \alpha_i \\ u \\ v \end{pmatrix} \quad (42)$$

The nonholonomic constraints also can be written as,

$$v_a \begin{pmatrix} \cos(\theta - \frac{\pi}{2}) \\ \sin(\theta - \frac{\pi}{2}) \end{pmatrix} = 0, \quad (43)$$

and,

$$v_d \begin{pmatrix} \cos(\theta + \alpha - \frac{\pi}{2}) \\ \sin(\theta + \alpha - \frac{\pi}{2}) \end{pmatrix} = 0 \quad (44)$$

Combining the six equations from (38) with (43) and (44) results in a system of eight equations and eight unknowns. Starting with zero initial conditions, these equations can be numerically integrated to solve for the configuration q and the Lagrange multiplier λ_1 and λ_2 .

We begin by solving (34) and (35) for u and v to obtain the result seen in Fig. 35 for the dimensions shown in Table 2. The plots in Fig 35 show the required value for u and v so that the point of contact of the steering wheel with the ground traces the same path as the wheel of the swivel car. The input to the revolute joint, α , is the steering angle shown in Fig. 35. To create a time dependency, we assume the swivel angle moves

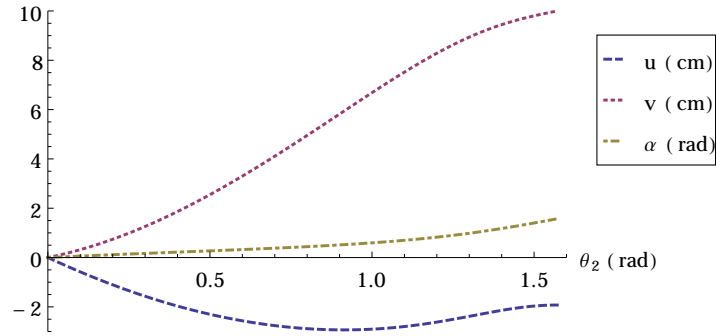


Figure 35: Changes in the input for u , v , and α versus the variation of the swivel joint

at a constant speed of $0.05 \text{ rad}\cdot\text{s}^{-1}$. The set of equations obtained from (38) are solved using Mathematica, from $t = 0$, to $t = 31.5$, at which the swivel angle reaches $\frac{\pi}{2}$. Fig. 36a, 36b, and 36c display how well the actuated joints, u , v , and α , follow the input using the inverse dynamic controller. Upon examining these figures, we can see how robust the inverse dynamic controller is at following a variable input, this means our system behaves similarly to the complete model. The effect of actuating the swivel joint on the x , z , and θ coordinates is shown in Fig 38. Furthermore, Fig. 37 shows the change in orientation and position of the simplified model as seen in Mathematica. Fig. 37a represents the swivel car at initial conditions. Whereas, Fig. 37d depicts the change in orientation and position of the swivel car when θ_2 reaches a value of $\frac{\pi}{2}$.

In agreement with our Dymola simulation, the car moves mostly backwards by 0.02 meters and the orientation changes by 0.2 radians in the clockwise direction. A similar motion was observed for MHT robot, where the mobile robot would slightly deviate from its current orientation when a single wheel is lifted at the beginning of the step climbing process.

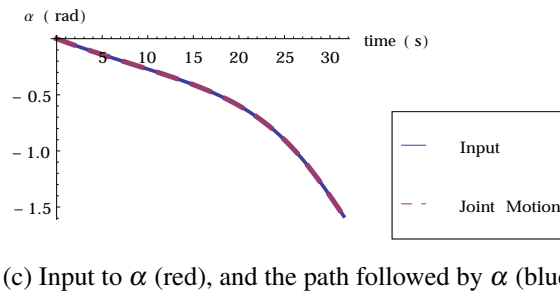
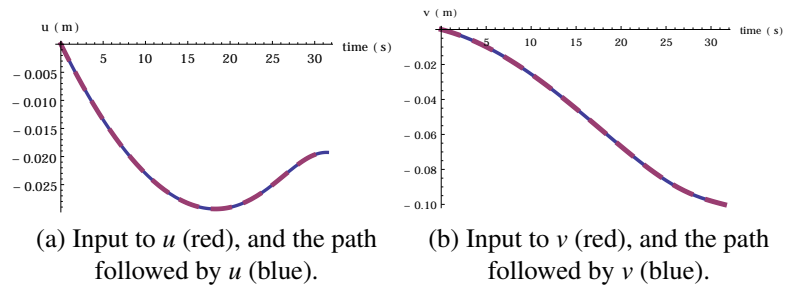


Figure 36: Input to each joint along with the output.

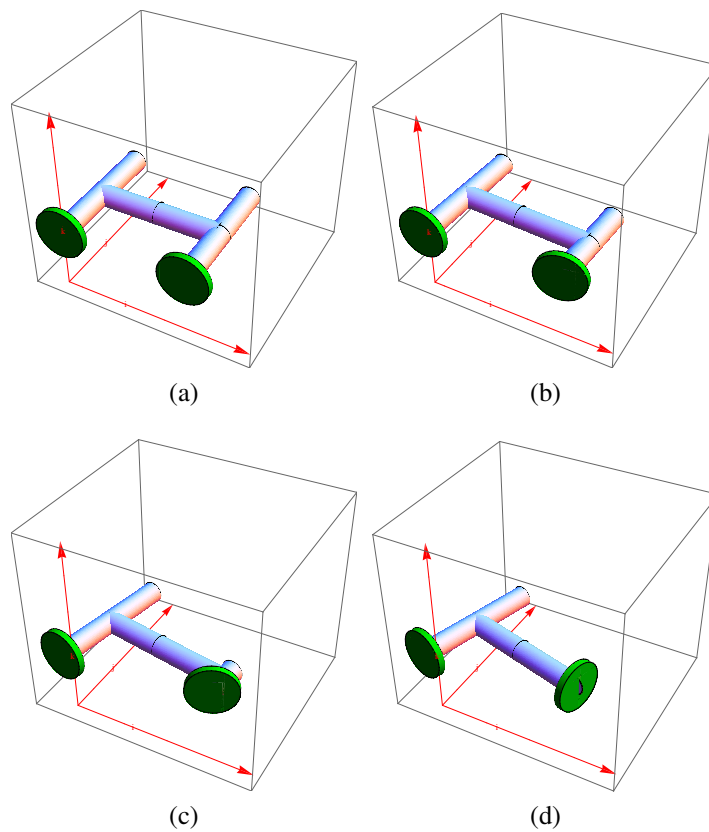


Figure 37: Change in pose of the swivel car starting from initial position, (a), and the final position of the swivel car when θ_2 reaches $\frac{\pi}{2}$, (d).

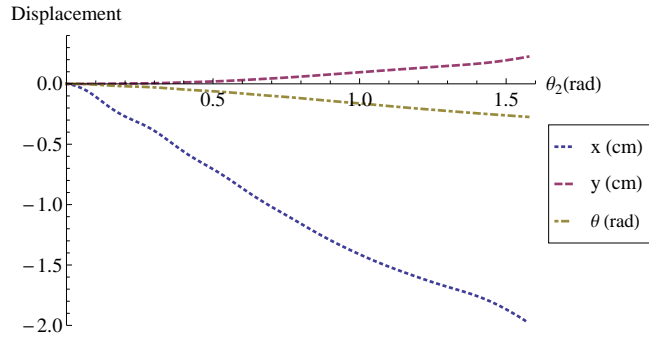


Figure 38: The effect of actuating the swivel joint on the position ,x and y, and the orientation θ

3. Effects of Varying Model Parameters

Now we investigate the effects of changing the model parameters on the dynamics of the simplified mechanism. We first investigate the effects of varying h on the dynamics of the simplified model. The simulation is first conducted for a wheel shaft length of $15cm$, and $20cm$, next we simulate our model for $\phi = \frac{\pi}{6}$, $\frac{\pi}{4}$, and $\frac{5\pi}{12}$. Finally, we run the simulation for $l = 30cm$ and $40cm$. By conducting all these simulations we aim to study the dynamics for different configurations of the swivel car. Table 3 illustrates the effects of varying the aforementioned parameters on the effects of actuating the twist joint. We notice than an increase in h is followed by increase in position and orientation change. However, an increase in ϕ decreases the effects of actuating the twist joint on the position and orientation of the mobile base. Finally, increasing l decreases the effects of actuating the twist joint on the pose of the robot.

Table 3: Effects of changing the design parameters on the robot's motion

Parameter	l	h	ϕ
Change in Parameter	↑	↑	↑
Effect of Twist Joint on Position	↓	↑	↓

E. Planar Motion Kinematics

In this part of section II, we derive the planar equations of motion for the proposed mobile robot by modeling it as a tricycle with an offset steering wheel. The model allows us to determine the angular and linear velocity of the mobile robot with respect to a ground frame given the angular velocity of the platform's wheels, and the value of the steering angle. These derivations can be used to implement closed loop motion and path planning in future work concerning the swivel car. Using the simplified

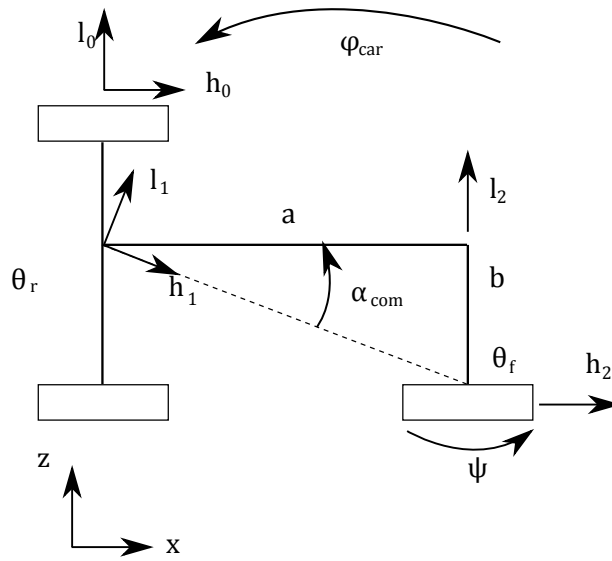


Figure 39: The simplified planar model of the swivel car resembles that of a tricycle with a variable offset steering wheel.

model implemented in the platform dynamics, we derive the kinematic equations of motion of the swivel car to determine the position and orientation given the steering angle and the rotation of the wheels. The simplified kinematic model is similar to that of a tricycle, but with an offset steering wheel as shown in Fig. 39. The system possesses five generalized coordinates $q_t = (x \ y \ \phi \ \theta_r \ \theta_f \ \psi \ a \ b)$. Similar to a regular tricycle [21], the vector q_t can be reduced to $q_t = (x \ y \ \theta_r \ \psi \ a \ b)$. The angular velocities of the rear wheel axis, the rear wheel and the front steering wheel are

$$\omega_c = \dot{\phi} \mathbf{k}, \quad (45)$$

$$\omega_r = \dot{\phi}_{car}\mathbf{k} + \dot{\theta}_r\mathbf{l}_0, \quad (46)$$

$$\omega_f = \dot{\phi}_{car}\mathbf{k} + \dot{\theta}_f\mathbf{l}_2 + \psi\mathbf{k}, \quad (47)$$

where ω_c is the angular velocity of the car in the XZ plane with respect to a fixed origin, ω_r is the angular velocity of the rear wheel with respect to the ground frame XZ , and ω_f is the angular velocity of the front wheel with respect to the XZ plane. With vectors

$$l_0 = \begin{pmatrix} -\sin \phi_{car} \\ \cos \phi_{car} \end{pmatrix}, \quad (48)$$

$$h_0 = \begin{pmatrix} \cos \phi_{car} \\ \sin \phi_{car} \end{pmatrix}, \quad (49)$$

$$l_2 = \begin{pmatrix} -\sin \phi_{car} + \psi \\ \cos \phi_{car} + \psi \end{pmatrix}, \quad (50)$$

$$h_2 = \begin{pmatrix} \cos(\phi_{car} + \psi) \\ \sin(\phi_{car} + \psi) \end{pmatrix}, \quad (51)$$

$$l_1 = \begin{pmatrix} -\sin(\phi_{car} + \alpha_{com}) \\ \cos(\phi_{car} + \alpha_{com}) \end{pmatrix}, \quad (52)$$

$$h_1 = \begin{pmatrix} \cos(\phi_{car} + \alpha_{com}) \\ \sin(\phi_{car} + \alpha_{com}) \end{pmatrix}, \quad (53)$$

with,

$$\alpha_{com} = \arctan \frac{b}{a} \quad (54)$$

The position of the rear wheel of the car, the front wheel, and the front wheel with respect to the rear wheel can be written as

$$C_r = P_r + r\mathbf{k}, \quad (55)$$

$$C_f = P_f + r\mathbf{k}, \quad (56)$$

$$C_f = C_r + c\mathbf{h}_1. \quad (57)$$

Deriving the above three equations with time yields

$$\dot{C}_f = r\dot{\theta}_f\mathbf{h}_2, \quad (58)$$

$$\dot{C}_r = r\dot{\theta}_r\mathbf{h}_0, \quad (59)$$

$$\dot{\theta}_f\mathbf{h}_2 = \dot{\theta}_r\mathbf{h}_0 + c\dot{\phi}_{car}\mathbf{l}_1 + \mathbf{h}_1f(a, b, \dot{a}, \dot{b}), \quad (60)$$

with

$$c = \sqrt{a^2 + b^2}, \quad (61)$$

$$f(a, b, \dot{a}, \dot{b}) = \frac{a\dot{a} + b\dot{b}}{\sqrt{a^2 + b^2}}. \quad (62)$$

Multiplying the third equation with l_f and l and solving for $\dot{\phi}$ yields,

$$\dot{\phi}_{car} = \frac{r\dot{\theta}_r \sin \phi_{car} + f(a, b, \dot{a}, \dot{b}) \sin (\psi - \alpha_{car})}{c \cos (\psi - \alpha_{car})}, \quad (63)$$

$$\dot{\phi}_{car} = \frac{r\dot{\theta}_f \sin \phi_{car} - f(a, b, \dot{a}, \dot{b}) \sin (\psi - \alpha_{car})}{c \cos \alpha_{car}}. \quad (64)$$

The two formulations, (64) and (63), represent the equation of the angular velocity of the robot in the XZ plane given the rear and front wheel velocity respectively. Due to the no slip condition placed at the robot's wheels, it is possible to determine the angular velocity of any wheel given the angular velocity of a single wheel. This means the angular velocity of the robot, $\dot{\phi}$, can be written either in terms of the rear wheel angular velocity, $\dot{\theta}_r$, or the front wheel angular velocity, $\dot{\theta}_f$ only.

The wheeled robot's motion is constraint such that both the front steering wheel and the rear driving wheels do not slip. These two constraint can be modeled mathematically by projecting the linear velocity of each wheel on both the x and z

direction, and equating these two values to zero [22, 23]. Mathematically, these two constraints can be written as,

$$\dot{x} \sin \phi_{car} + \dot{y} \cos \phi_{car} = 0, \quad (65)$$

and,

$$-\dot{x} \sin (\phi_{car} + \psi) + \dot{y} \cos (\phi_{car} + \psi) + \sqrt{a^2 + b^2} \dot{\phi}_{car} \cos (\psi - \alpha_{com}) = 0. \quad (66)$$

Solving these two equations and substituting for the value of ϕ derived in (64), the mobile robot's velocity in the x and y direction can be written as,

$$\dot{x} = r \dot{\theta}_r \cos \phi_{car}, \quad (67)$$

and,

$$\dot{y} = r \dot{\theta}_r \sin \phi_{car} \quad (68)$$

Note that (67) and (68) are similar to the equations of a car-like robot, however due to the kinematics of the swivel car, some compensation is required to account for the dynamic effects of actuating the swivel car. The equations shown above are non integrable equations. However they can be solved by implementing a finite time difference as shown below,

$$x_{t+1} = \Delta t \dot{x} + x_t \quad (69)$$

$$y_{t+1} = \Delta t \dot{y} + y_t \quad (70)$$

$$\phi_{t+1} = \Delta t \dot{\phi} + \phi_t \quad (71)$$

Solving (69), (70) and (71) for a constant steering angle of $\frac{\pi}{6}$, a constant angular velocity of 0.1 rad.s^{-1} for the rear wheel, and a constant time step of 0.1 seconds, we get the plot shown in Fig. 40.

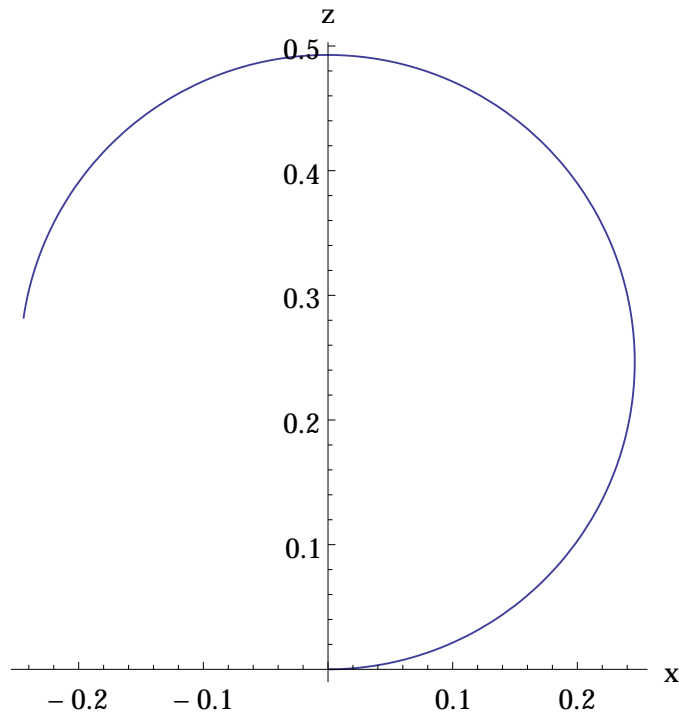


Figure 40: The path followed by solving the equations of motion (67) and (68).

F. Parameter Study

In this part of chapter II, we study the effects of varying the design parameters on the effectiveness of the proposed mobile base. In what follows, we study the advantages and disadvantage of varying each parameter. Furthermore, we investigate possible relationships and constraints between the design parameters. So far, the proposed mobile base may face these two problems;

1. The car might tip over due to its high center of gravity.
2. The steering wheel might touch the rear wheels.

In what follows, we propose some simple rules-of-thumb to prevent the two problems mentioned above, then we proceed to discuss the advantages and disadvantages of varying each parameter.

1. Rules of Thumb for Parameter Selection

We begin by solving the first problem. The robot is prone to tipping over if its center of, C_m moves behind the rear wheel axis as shown in Fig. 41. Mathematically, this relationship can be expressed as,

$$\frac{\phi}{2} + \theta_1 < \frac{\pi}{2} \quad (72)$$

To avoid the problem of tipping over, the value of θ_1 must never exceed $\frac{\pi-\phi}{2}$ for all applications.

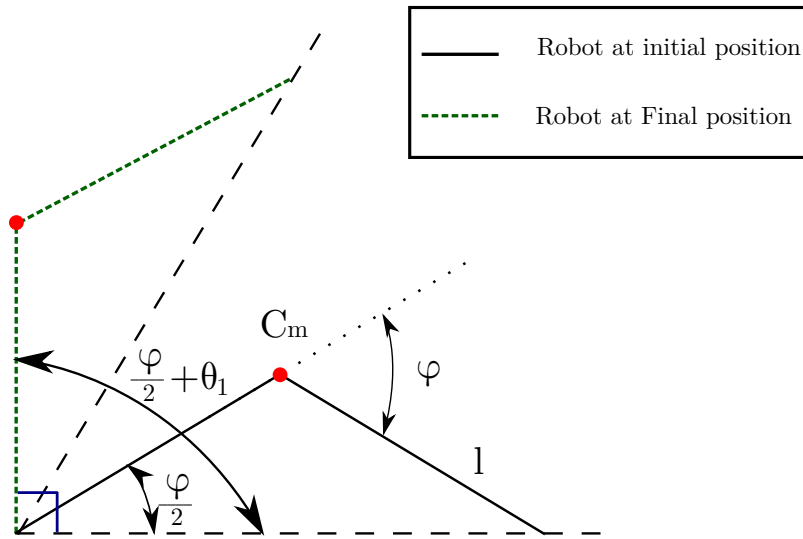


Figure 41: A simple representation of the swivel at its initial position and at the position just before the mobile base tips over

The second problem results when the length of the wheel shaft axis is too large, when ϕ is too large, or when the length of the “T” column l is small. As a result the front steering wheel might touch the rear wheels and cause the car to stall. Meaning the projection of the length of the wheel shaft, h , on the ground plane must always be less the projection of the car’s length on the ground plane. Referring to Fig. 42, the projection of both these lines of the ground plane, l_p and h_p are,

$$l_p = 2l \cos \frac{\phi}{2} \cos \theta_1, \quad (73)$$

and

$$h_p = h \sin \frac{\pi}{2} - \phi \quad (74)$$

Combing (73) and (74) yields the relationship shown below,

$$h_p = h \sin \frac{\pi}{2} - \phi < l_p = 2l \cos \frac{\phi}{2} \cos \theta_1. \quad (75)$$

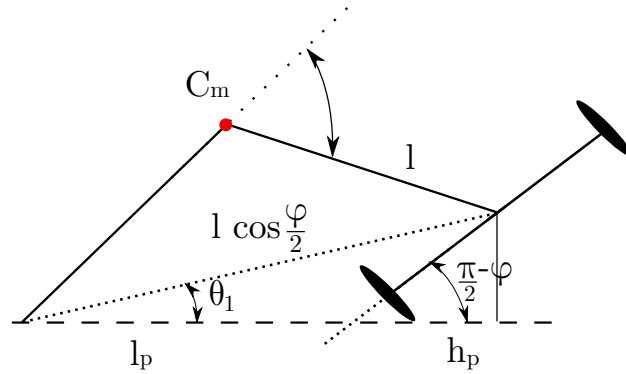


Figure 42: A simple representation of the swivel car along with its steering shaft at a twist angle of $\frac{\pi}{2}$

2. Effects of Varying The Design Parameters

Changing the value of a design parameter can greatly effects the kinematics and dynamics of the swivel car. This was demonstrated in previous sections, for h and ϕ in particular, but not fully studied. In what follows, we briefly discuss the effects of changing the robot's design parameters, l , h and ϕ .

a. The Angle ϕ

Changing ϕ effects the car's steering capabilities and the peak torque required at the twist joint to steer. An increase in ϕ increases steering capabilities as shown in Fig. 21a. Furthermore, increasing ϕ decreases the torque required to steer the car. However,

increasing ϕ decreases the mobile robot's climbing capabilities. Moreover, if h is large enough, increasing ϕ can cause the front steering wheel to touch the rear wheel axis.

b. Steering Wheel Shaft Length

Increasing h improves the swivel car's climbing capabilities. However this change increases the risk of tipping over, the risk of the front wheels stalling with the rear wheels while steering, the torque required at the twist joint, and the effects of actuating the twist joint on the position of the car.

c. "T" Column Length

For a small value of l , the swivel car is at risk of tipping over due to its relatively small length. However, increasing l can decrease the effects of actuating the twist joint on the position and orientation of the swivel car with respect to the ground plane.

CHAPTER III

STEP CLIMBING ALGORITHM

In Section III, we propose two simple step climbing procedures for the swivel car based on the car's kinematics and dynamics. The first step climbing procedure was developed for a positive value of ϕ , whereas the second process only works when ϕ is negative. The need for two procedures stems from the difference in kinematic behavior of the mobile platform when the parameter, ϕ changes sign as shown in Section II. The aim of both procedures is to lift the front wheels of the swivel car above a certain step. When this occurs, we can assume the mobile platform has overcome the step [2].

A. For a Positive ϕ

In this part of Section III, we propose a step climbing procedure for a swivel car configuration with positive ϕ . For this analysis to work, we assume that the following parameters are known: the distance from the robot to the step, d , the height of the step, h_s , and the orientation of the step with respect to the swivel car, θ_i .

In our proposed step climbing technique, the swivel steering platform will traverse a series of motions, namely, arcs and straight lines [22], to place the bottom of the lifted wheel on top of the obstacle as shown in Fig. 43. We have to take into account the dynamics of the platform, since during the actuation of the swivel angle, i.e., steering, the platform changes position and orientation.

To find the distance, d , we first determine the value of the steering radius, R , shown in Fig. 44

$$R = \frac{2l \cos \phi}{\tan \alpha}, \quad (76)$$

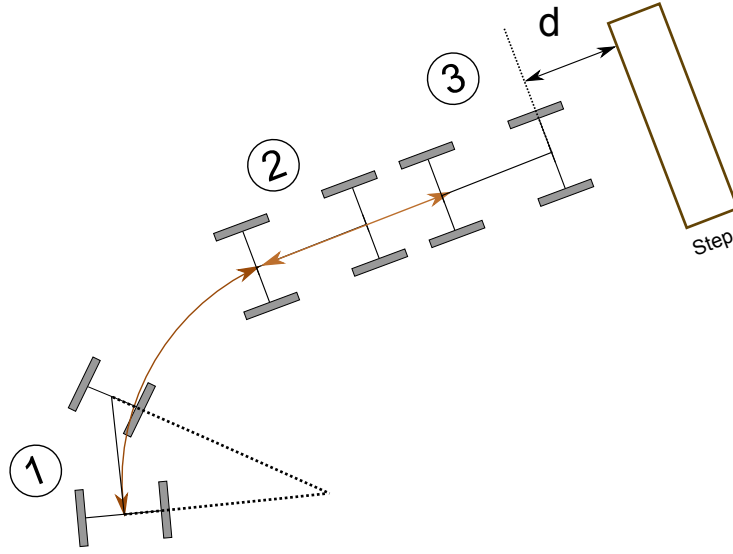


Figure 43: The swivel car positioning itself to climb a step

where α is the steering angle. Through trigonometry, the steering radius for the front of the robot R' is,

$$R' = \frac{R}{\cos \alpha}. \quad (77)$$

Substituting (76) into (77) yields,

$$R' = \frac{2l \cos \phi}{\sin \alpha}. \quad (78)$$

The steering radius of the lifted wheel, R_2 , is,

$$R_2 = R' + h - v. \quad (79)$$

Plugging (78) into (79) yields,

$$R_2 = \frac{2l \cos \phi}{\sin \alpha} + h - v \quad (80)$$

Since, d' and d'' are chords within circles of radii R' and R'' , they can be written

as

$$d' = 2R' \sin \frac{\delta\theta_i}{2}, \quad (81)$$

and

$$d'' = 2R_2 \sin \frac{\delta\theta_i}{2}, \quad (82)$$

where $\delta\theta_i$ is the arc angle shown in 44 and can be written as,

$$\delta\theta_i = \theta_i - \gamma, \quad (83)$$

where γ is the orientation of the step with respect to the swivel car at the end of the step climbing process.

Utilizing the Sine law for the triangle with sides d and d'' the following relationship can be obtained,

$$d_2 = \frac{d'' \sin \gamma}{\sin(\pi - \theta_i)}. \quad (84)$$

Finally, substituting (82) into (84) yields,

$$d = 2R_2 \sin \frac{\delta\theta_i}{2} \tan \gamma + (h - v) \cos \left(\frac{\pi}{2} - \alpha \right) \quad (85)$$

Upon close examination, we notice that (85) is dependent only on the twist angle, θ_2 , which in turn depends on the height of the faced obstacle. The required twist angle to scale a step was previously determined in chapter II and can be used in this climbing algorithm. Hence, our step climbing technique can be summarized as follows: given the step height, h_i , and the direction of the lifted wheel with respect to the step, γ , we first solve for the swivel angle θ_2 . Then, solve for the distance, d , and the orientation of the platform with respect to the obstacle, θ_i . The solved values for d and using (85) guarantee that as the robot drives forward, the lifted wheel clears the obstacle and touches its top with an orientation γ . The climbing algorithm was implemented using the software Webots for validation as shown in Fig. 45.

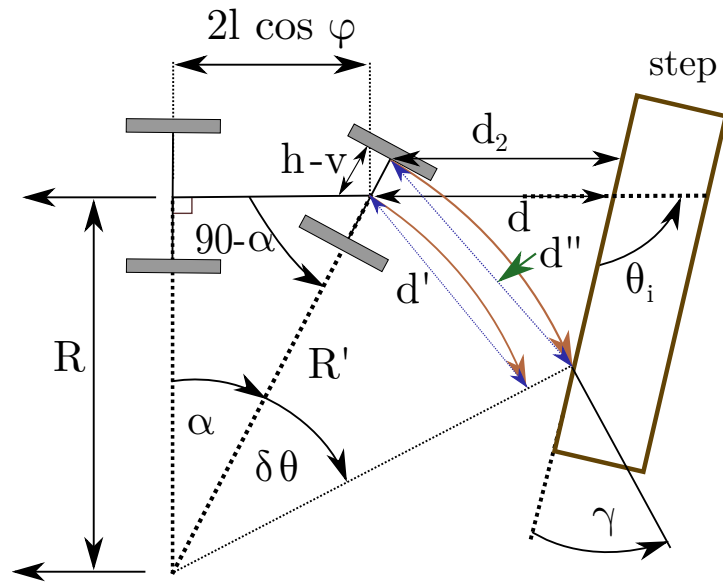


Figure 44: Variables taken into account during the step climbing process

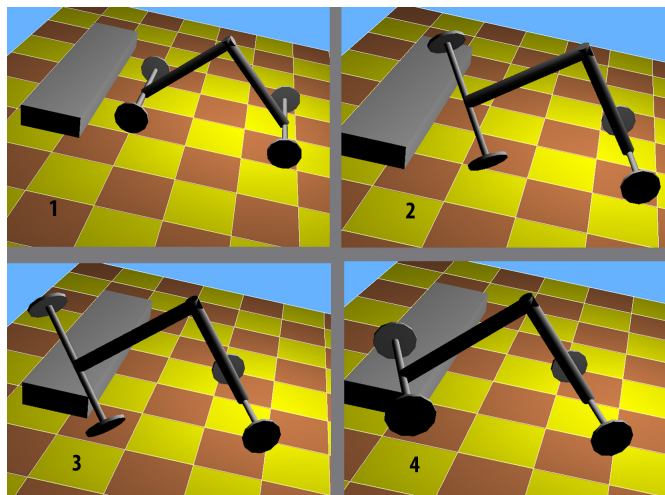


Figure 45: Implementation of the step climbing procedure

B. For a Negative ϕ

For a negative value of ϕ , it is possible to create a semi-active step climbing process based on the kinematics of the proposed mobile base, and its mechanical configuration. The mobile platform approaches the step at a certain angle, θ_i , until its front wheel is in contact with the step. Once the front wheel hits the step, the car uses its inertia, driving torque, and the torque at the swivel joint to lift its front wheel above the

step. This method decreases the peak torque at the swivel joint to lift the front wheel and eliminates the need for complex calculations. This procedure was labeled semi-active because, with a large enough driving torque at the wheels, it is possible to lift one wheel above an obstacle without exerting any torque at the swivel joint. Fig. 46 illustrates the point at which the force is applied and the resulting torque which is induced about the twist joint.

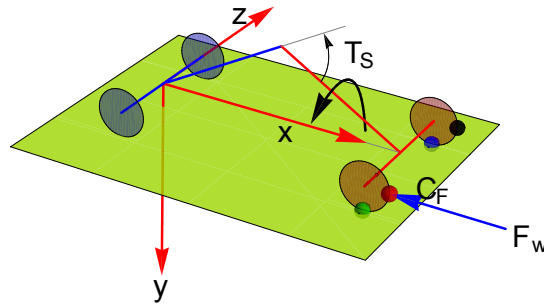


Figure 46: A skeletal diagram representing the forces and torques about the swivel joint when the front wheel is in contact with a step.

Due to the proposed design of the swivel car, a force applied at a single wheel creates a torque at the wheel shaft, h , about its respective “T” column. However, the sign of ϕ changes the direction in which the “T” column rotates. When ϕ is negative, the resulting torque helps lift the wheel which is in contact with the obstacle. On the other hand, when ϕ is positive the resulting torque pushes the wheel down. Fig. 46 depicts the point of application of this force, and the axis about which torque is generated.

1. Force Analysis for Procedure

We begin by presenting a simple force analysis to determine the torque produced when the front wheel is in contact with an obstacle. The car's driving torque, τ_D , at the wheels creates a forward driving force, F_w . When a wheel is in contact with an obstacle, the resulting reaction force is equal to the driving force, F_w . This reaction force

is projected along the base of the “T” column, and the F_{NT} direction as shown in Fig. 47.

The force, F_w can be calculated from the driving torque as,

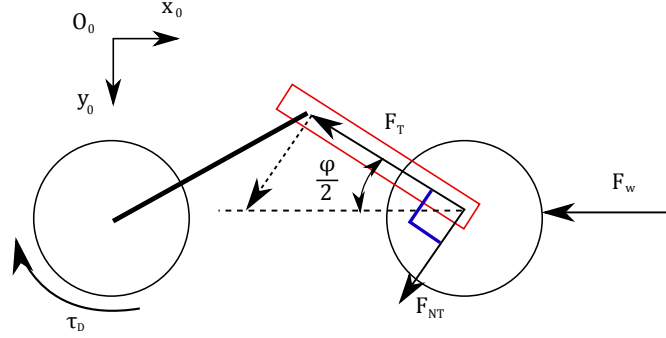


Figure 47: A free body diagram showing the forces acting on the swivel car.

$$F_s = \tau_D r, \quad (86)$$

where r is the radius of the wheel. Using simple trigonometry, F_w is then decomposed into two perpendicular forces, F_T , and F_{TN} . Where F_T is the projection of F_w along the base of the “T” column as shown in Fig. 47. Considering the right triangle ABC , F_T and F_{TN} can be written as

$$F_T = F_w \cos \frac{\phi}{2}, \quad (87)$$

and,

$$F_T = F_w \sin \frac{\phi}{2}. \quad (88)$$

The torque about the “T” column resulting from the force, F_{TN} , can be determined as,

$$\tau_S = h F_{NT}, \quad (89)$$

where h is the wheel shaft length shown in Fig. 16. Examining (88), we notice that for a positive ϕ , the resulting torque, τ_S , pushes the front wheel in contact with the step towards the ground. However, when ϕ is negative, the resulting force normal to the “T” column is upwards, consequently the generated torque, τ_S , pushes the front wheel upwards. Fig. 46 depicts a skeletal model of the swivel car with the direction of the

reaction force, and the location of the torque resulting from this force.

We solve (89) for different values of h and r to determine the effects of changing the cars parameters on the value of τ_S given the driving torque, τ_D . Fig. 48 and 49 display the variation of the torque for different values of h and r the moment when the front wheel is in contact with the step.

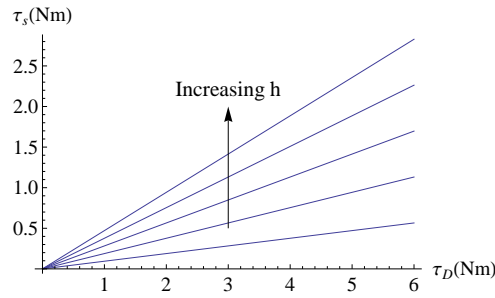


Figure 48: Driving torque, τ_D , versus induced torque, τ_S for $h = (1, 2, 3, 4, 5)$

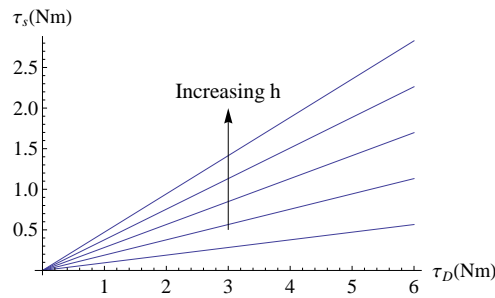


Figure 49: Driving torque, τ_D , versus induced torque, τ_S for $h = (0.5, 0.7, 0.9, 1.1, 1.3)$

So far we presented the magnitude of the assisting torque that is generated at the swivel joint when the front wheel is in contact with the step. In reality, this value changes as the swivel angle changes, and becomes zero when the front wheel reaches the top position, i.e. θ_2 is $\frac{\pi}{2}$. For this analysis we must take into account two variables that effect the torque produced at the joint. The first variable is the distance from the point of application of F_S , to the swivel joint. As the swivel joint is actuated, this distance decreases and as a result, the assisting torque also decreases. the second variable is the change in orientation of the wheel shaft, h . As the swivel joint is actuated, the projection of h on the XZ plane changes orientation. This means a smaller amount of force can be utilized to help actuate the swivel joint.

$$\alpha_c = \theta - \frac{\pi}{2} \quad (90)$$

$$h_p = h \sin(\phi - \theta_1) \cos \theta_2 \quad (91)$$

Implementing (91), we can determine the effect of actuating the swivel joint, θ_2 on the assisting torque, τ_S . Fig. 50 and 50 depict this relationship for different values of the parameters, h and r . We notice that increasing r actually decreases the value of the assisting torque. However, increasing h actually increases the value of τ_S . Furthermore, upon examining these two figures, we notice an increase in the assisting torque s θ_2 increases.

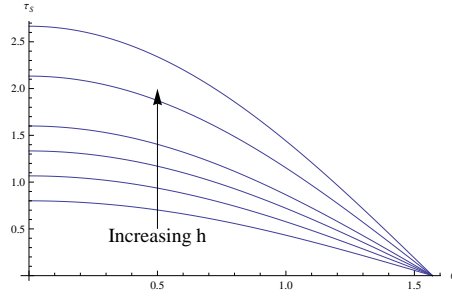


Figure 50: Induced torque, τ_S , vs. the change in the swivel angle, θ_2 for $h = (0.5, 0.7, 0.9, 1.1, 1.3)$

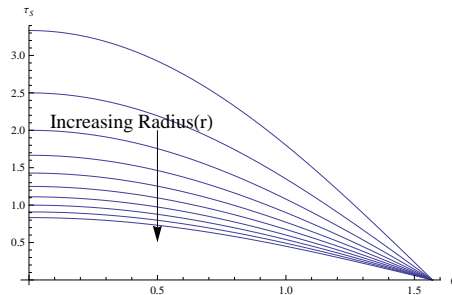


Figure 51: Induced torque, τ_S , vs. the change in the swivel angle, θ_2 , for $h = (0.5, 0.7, 0.9, 1.1, 1.3)$

The values of τ_S shown in Fig. 50 and 51 are relatively small compared to the peak torque requirements determined in Section II. However, it should be noted that we overestimated the weight of the swivel car for comparison with some experiments

conducted in literature. Hence, if we assume the car weighs almost 10 kg , and the length of the wheel shaft, h , is around 5 cm , an assisting torque starting at 2.5 Nm can be helpful when climbing a step.

2. Kinematic Analysis of the Step Climbing Process

When climbing a step using this method, care should be taken to prevent the steering wheel C_S from touching the step as it can prevent the mobile platform from overcoming the step. When ϕ is negative, this issue becomes problematic since the steering wheel moves away from the rear wheel axis and towards the step when the swivel joint is actuated. This was previously demonstrated in Section II when analyzing the path of the point of contact, p .

This problem can be prevented by controlling the approach angle, α_{AP} (shown in Fig. 52), and preventing it from dropping below a certain value. The minimum value is determined by calculating the angle formed by the face of the step, PL_1 , and the surface, PL_2 , perpendicular to the XZ plane, and containing the two point, C_F and P_l . Where C_F is the furthest point from the reference frame, O_0 , on the steering wheel measured along the x_0 direction. And P_l is the lowest point lying on the circumference of the lifted wheel. Fig. 53 depicts the planes and points mentioned above and their respective position with respect to the swivel car.

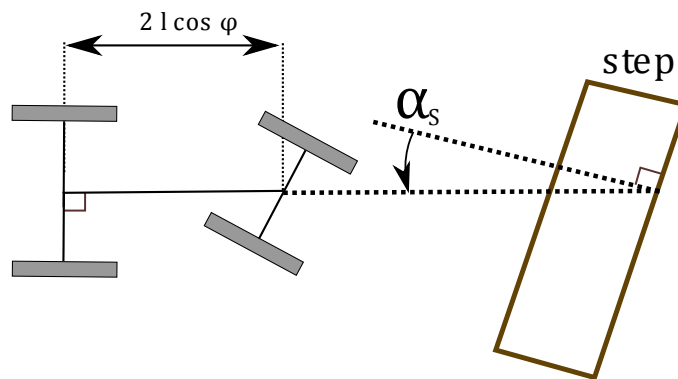


Figure 52: Approach angle α_{AP}

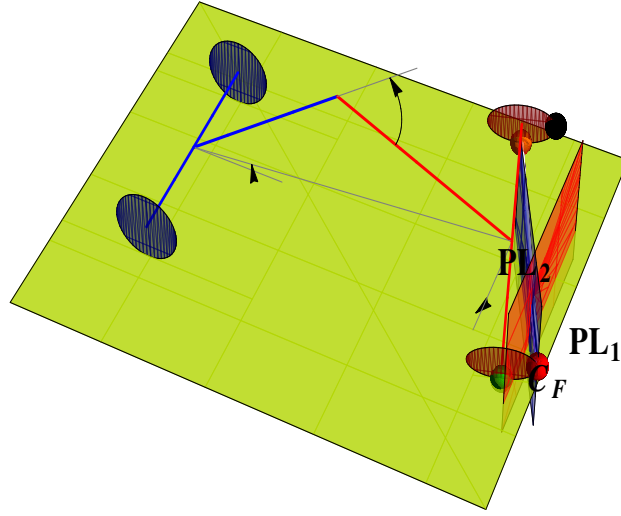


Figure 53: Skeletal representation of the swivel car showing the intersection of the step's surface with the plane formed by the two points, C_F and P_L .

The position of P_L , X_{PL} and Z_{PL} , in the XZ plane can be written as,

$$\begin{aligned}
 X_{PL} = \frac{1}{4} & \left(4l \cos\left(\theta_1 - \frac{\phi}{2}\right) + 2h \cos\left(\theta_1 - \theta_2 - \frac{\phi}{2}\right) - 2h \cos\left(\theta_1 + \theta_2 - \frac{\phi}{2}\right) \right. \\
 & + 4l \cos\left(\theta_1 + \frac{\phi}{2}\right) + 2r \cos(\theta_1 - \theta_3) + r \cos(\theta_1 - \theta_2 - \theta_3) \\
 & + r \cos(\theta_1 + \theta_2 - \theta_3) + 2r \cos(\theta_1 + \theta_3 - \phi) \\
 & \left. - r \cos(\theta_1 - \theta_2 + \theta_3 - \phi) - r \cos(\theta_1 + \theta_2 + \theta_3 - \phi) \right), \quad (92)
 \end{aligned}$$

and,

$$Z_{PL} = h \cos \theta_2 + r \left(-\cos \frac{\phi}{2} \sin \theta_2 \sin \theta_3 + \cos \theta_3 \sin \theta_2 \sin \frac{\phi}{2} \right) \quad (93)$$

Substituting the solution derived in (16) into (92) and (93) yields the position of P_L in the XZ plane for different values of θ_2 . Fig. 54 depicts the path followed by P_L in the XZ plane starting at $\theta_2 = 0$ till $\theta_2 = \frac{\pi}{2}$. The red dot in this figure is the initial position of P_L when $\theta_2 = 0$.

The position of C_F in the XZ is determined in a similar fashion to that of P_L .

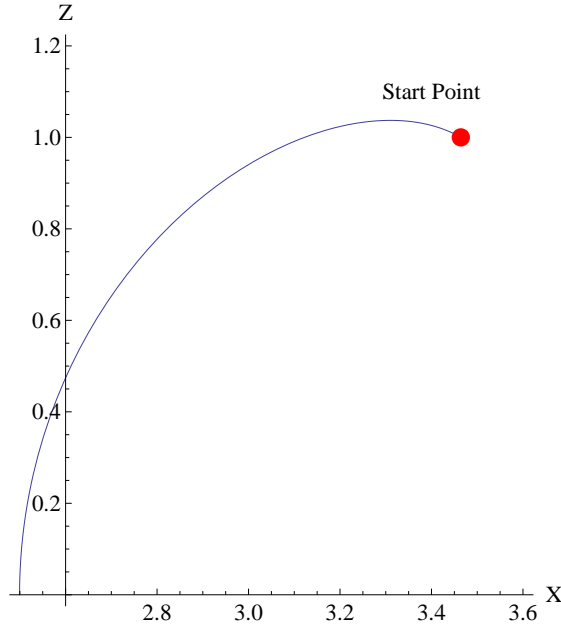


Figure 54: Change in position of P_L in the XZ plane when θ_2 varies from 0 to $\frac{\pi}{2}$

Starting from the O_3 reference frame shown in Fig. 16, we perform the following transformation:

1. Rotation about the z_3 axis by an angle of $\frac{\phi}{2}$.
2. Rotation about the z_3 axis by an arbitrary angle θ_3 .
3. Translate about the new x-axis by a distance r .

By performing the transformations above, we obtain the coordinates of an arbitrary point, P_{R2} about the circumference of the steering wheel, D . The position of this point in the XZ plane can be written as,

$$\begin{aligned}
 X_{P2} = & \frac{1}{4} \left(4l \cos \left(\theta_1 - \frac{\phi}{2} \right) - 2h \cos \left(\theta_1 - \theta_2 - \frac{\phi}{2} \right) + 2h \cos \left(\theta_1 + \theta_2 - \frac{\phi}{2} \right) + 4l \cos \left(\theta_1 + \frac{\phi}{2} \right) \right. \\
 & + 2r \cos(\theta_1) + r \cos(\theta_1 - \theta_2) + r \cos(\theta_1 + \theta_2) + 2r \cos(\theta_1 - \phi) \\
 & \left. - r \cos(\theta_1 - \theta_2 - \phi) - r \cos(\theta_1 + \theta_2 - \phi) \right), \tag{94}
 \end{aligned}$$

and,

$$Z_{P2} = -h \cos \theta_2 - r \sin \theta_2 \sin \left(\theta_3 - \frac{\phi}{2} \right). \tag{95}$$

To determine the position of point C_F , we derive (95) with respect to θ_3 and equate the resulting equation to zero,

$$\frac{\partial X_{P2}}{\partial \theta_3} = 0. \quad (96)$$

Solving (96) we get,

$$\theta_{3sol2} = -\arccos\left(\sin\frac{\phi}{2}\right) \quad (97)$$

Substituting (97) into (94) and (95) yields the position of C_F in original coordinate frame, O_0 . Fig. 55 displays the change in position of C_F in the XZ plane for different values of θ_2 .

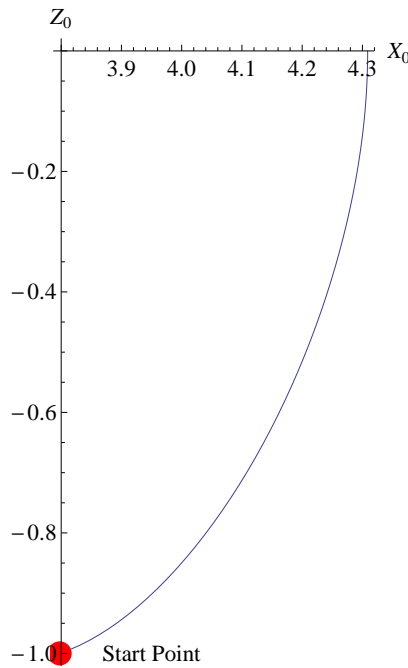


Figure 55: Change in position of C_F in the XZ plane when θ_2 varies from 0 to $\frac{\pi}{2}$

The change in position of both P_l and C_F with respect to the initial ordinate frame, O_0 , is illustrated in Fig. 56. These two points form an angle, α_S , with the projection of PL_1 on the XZ plane.

The angle, α_S , formed by the face of the step and projection of the line $P_l C_F$ on the XZ , can be calculate by using the definition of the dot product. We begin by

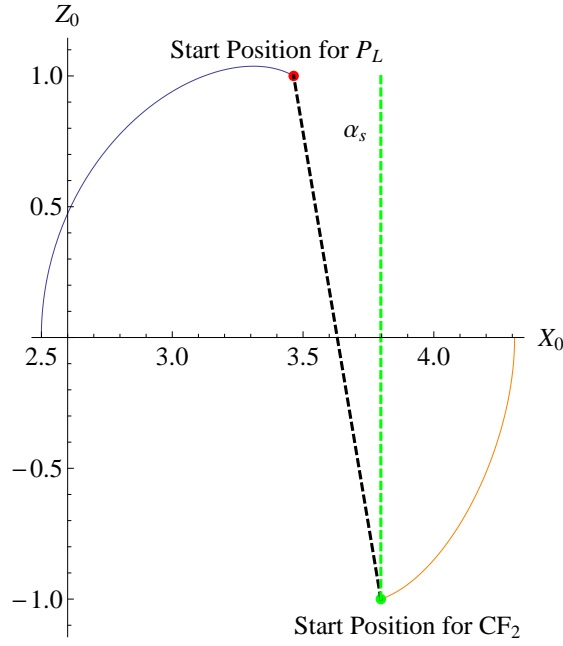


Figure 56: Change in position of P_L and C_F in the XZ plane with respect to the origin O_0 .

calculating the unit vector, $vecl_{PL}$ along the line $P_L C_F$.

$$\mathbf{l}_{PL} = \begin{pmatrix} \frac{X_{PL} - X_{CF}}{\sqrt{(X_{PL} - X_{CF})^2 + (Z_{PL} - Z_{CF})^2}} \\ \frac{Z_{PL} - Z_{CF}}{\sqrt{(X_{PL} - X_{CF})^2 + (Z_{PL} - Z_{CF})^2}} \end{pmatrix} \quad (98)$$

The projection of PL_1 on the XZ plane is a line parallel to the z_0 axis, consequently the unit vector along this line, \mathbf{l}_{PL1} can be written as,

$$\mathbf{l}_{PL1} = \begin{pmatrix} 0 \\ 1 \end{pmatrix}. \quad (99)$$

Using the definition of the dot product and substituting (98) and (99) into this definition, we calculate the value of the approach angle, α_S ,

$$\alpha_S = \arccos \frac{\mathbf{l}_{PL1} \cdot \mathbf{l}_{PL}}{\|\mathbf{l}_{PL}\| \cdot \|\mathbf{l}_{PL1}\|}. \quad (100)$$

Equation (100) is solved for the dimensions shown in Table 2, with θ_2 being varying from 0 to $\frac{\pi}{2}$. Plots depicting the needed approach angle, α_s , vs. the swivel angle and the height of the step are shown in Fig. 57 and 57. Fig. 57 depicts the minimum approach angle needed to climb a step while preventing the steering wheel from making contact with the face of the step, PL_1 . Moreover, Fig. 58 displays the minimum required approach angle to prevent interference from the steering wheel given the height of the step.

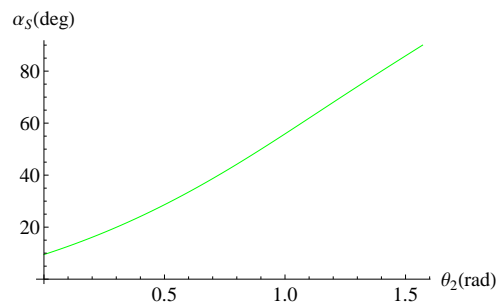


Figure 57: Minimum value required for the approach angle to overcome a step without interference from the steering wheel.

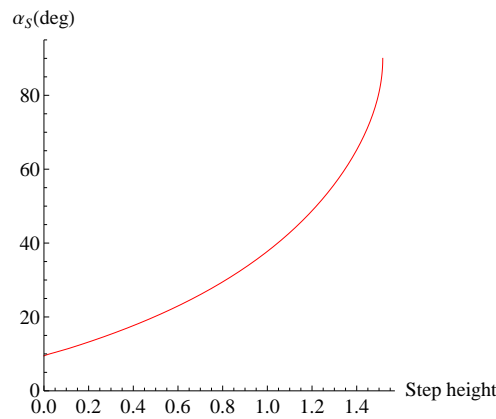


Figure 58: Minimum value required for the approach angle to overcome a step of certain height, without interference from the steering wheel.

When ϕ is negative, the swivel car can use the driving torque to overcome steps in a semi active manner. However to do so, the swivel car must approach a step at a specified angle to prevent the steering wheel from touching the face of the step.

CHAPTER IV

COMPARISON TO OTHER MOBILE PLATFORMS

In this section, we compare the step climbing capabilities of the swivel car to other mobile robots of similar dimensions. First we begin by comparing the climbing capabilities of our proposed design to a car-like robot. Afterwards, we compare the swivel to other mobile robots designed to climb steps and obstacles.

A. Normal Vehicles

We now analyze the step climbing dynamics of a car-like robot using the Euler-Lagrange formulation. This is done to determine the peak torque requirement and the expended energy to lift the base of its front wheel above the step. A normal vehicle, such as a car, is unable to climb steps higher than half its wheel diameter [2]. However, with an actuator large enough some mobile vehicles can climb steps slightly smaller than half the wheel diameter. This procedure can be modeled as a slider-crank mechanism with an offset slider [2, 24] as seen in Fig. 59, however instead of applying torque at the base of the crank, the torque is applied at the crank pinion [2, 25]. To further simplify the system, we assume the entire mass of the car, m_b is located at the center of gravity, C_{car} . The system is modeled using the Euler-Lagrange formulations with generalized coordinate vector $q = (x \ y \ \theta_w \ \alpha_b)$. The kinetic energy and potential energy of the system are

$$T = 0.5m_b(v_x^2 + v_y^2) + 0.5I_{cm}\dot{\alpha}_b^2, \quad (101)$$

and

$$V = m_b g (R_w \sin \theta_w - c_x \sin \alpha_b + c_y \cos \alpha_b). \quad (102)$$

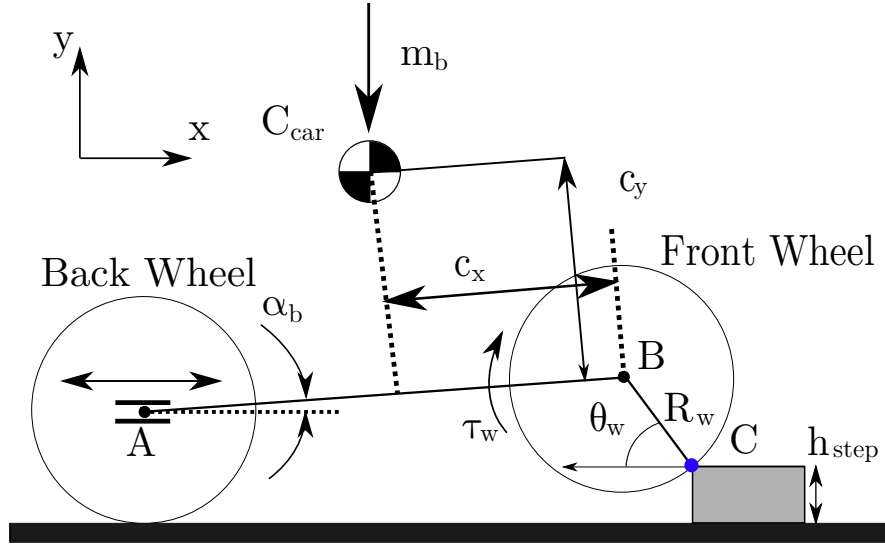


Figure 59: The crank-slider mechanism used to model the climbing process of a car-like robot

The two velocities of the center of mass, C_{car} , v_x and v_y can be written as

$$v_x = (-c_y \cos \alpha_b + c_x \sin \alpha_b) \dot{\alpha}_b - R_w \sin \theta_w \dot{\theta}_w, \quad (103)$$

and

$$v_y = -c_x \cos \alpha_b \dot{\alpha}_b - c_y \sin \alpha_b \dot{\alpha}_b + R_w \cos \theta_w \dot{\theta}_w. \quad (104)$$

Substituting (103) and (104) into (101) and (102) we get

$$T = \frac{I_{cm} \dot{\alpha}_b^2}{2} + \frac{m_b}{2} \left((-c_x \cos \alpha_b \dot{\alpha}_b - c_y \sin \alpha_b \dot{\alpha}_b + R_w \cos \theta_w \dot{\theta}_w)^2 + (-c_y \cos \alpha_b \dot{\alpha}_b + c_x \sin \alpha_b \dot{\alpha}_b - R_w \sin \theta_w \dot{\theta}_w)^2 \right) \quad (105)$$

and

$$V = gm_b(c_y \cos \alpha_b - c_x \sin \alpha_b + R_w \sin \theta_w), \quad (106)$$

where m_b is the mass of the car and I_{cm} is the inertia of the center of mass about the rear wheel. The Lagrangian is

$$L = T - V. \quad (107)$$

Table 4: Simulation parameters for car-like robot

Parameter	Value	Label
m_b	21 Kg	Car Mass
I_{cm}	1.96 Kg.m ²	Inertia of C_{car} about rear wheel axis
c_x	0.215 m	Position of C_{car} in x-direction
c_y	0.25 m	Position of C_{car} in y-direction
b	0.43 m	Length of the car body
R_w	0.075 m	Wheel Radius
h_{step}	16 mm	Height of the step
K_p	7.6	Proportional Gain

Like any crank-slider, any change in the angle α_b is followed by a change in the crank angle, θ_w . This constraint can be written as,

$$\alpha_b = \arcsin \frac{(R_w \sin \theta_w - R_w + h_{step})}{b}. \quad (108)$$

By substituting the value of v_x , v_y , and α , it is possible to write the Lagrangian in terms of one variable, θ_w , and its derivatives, $\dot{\theta}_w$ and $\ddot{\theta}_w$. The resulting Euler-Lagrange equation is

$$\frac{d}{dt} \left(\frac{\partial L}{\partial \dot{q}} \right) - \frac{\partial L}{\partial q} = K_p(\theta_g - \theta_w), \quad (109)$$

where K_p is a proportional gain, θ_g is the goal angle (usually $\frac{\pi}{2}$), and θ is the current angle. The term $K_p(\theta_g - \theta_w)$ is used to control the position of the angle θ_w by controlling the torque, τ_w , applied about point B . The system is solved in Mathematica using the parameters of Table 4. The energy expended is

$$E = \int_0^t \dot{\theta}_w \tau_w dt, \quad (110)$$

where τ_w is the torque at the crank pin, and $\dot{\theta}_w$ is the angular velocity of the crank. To verify the results achieved in Mathematica, another simulation was conducted in Dymola using the multibody library. Both simulations gave the same result. Referring to Fig. 60 and 61, the peak torque required to climb a step 12mm high is 6.5 Nm, and the energy expended during the climbing process is 3.2 J. Compared to the dynamic simulations

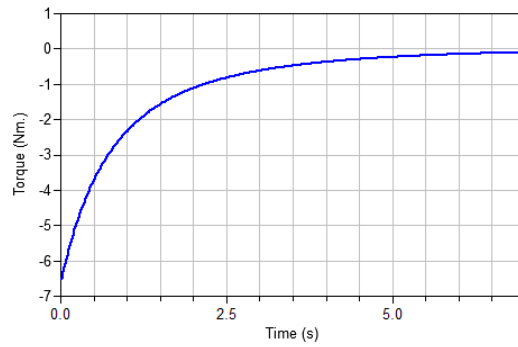


Figure 60: Torque variation with time of the step climbing process

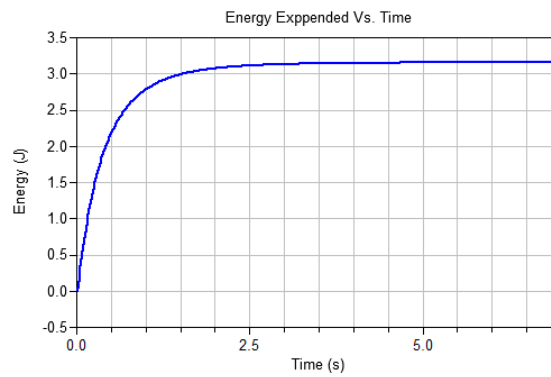


Figure 61: Energy consumption of the step climbing process vs. time

conducted in Section II, the swivel car requires a higher peak torque to climb a step of similar height. Furthermore, both mobile vehicles expend the similar amounts of energy while climbing a step. On the other hand, the swivel car posses superior step climbing capabilities as it can climb steps larger than the diameter of its wheels. Moreover, the swivel car posses better steering capabilities than a regular car-like robot. Whereas a car-like robot is unable to achieve a steering angle of $\frac{\pi}{2}$ mainly due to the use of Ackerman steering, the swivel car is capable of rotating about its own axis.

B. Other Mobile Robots with Climbing Capabilities

In the final part of this section, we compare the step climbing capabilities of the swivel car with some of the other mobile platforms mentioned in the introduction. For simplicity, comparison is based on the maximum scalable step given the size of the

wheels for each platform. Unlike the car-like robot which cannot climb steps higher than half its wheel diameter, the swivel car is shown to climb steps almost as high as its wheels. Consequently, when compared to a car-like robot of the same dimensions, the swivel car possesses superior step climbing capabilities, but requires a larger actuator to climb steps. However, when compared to Genbu and SHRIMP, a swivel car of similar dimensions can climb steps 20 percent larger than its wheel diameter versus 10 percent for Genbu and 200 percent for SHRIMP. Even though our proposed mobile base is better than Genbu, it is not as good as SHRIMP which can climb larger steps and does not require a controlled procedure to climb steps. For a swivel car with dimensions similar to Rocky 7, the former can climb an obstacle almost twice as high as its wheel diameter, whereas Rocky 7 can climb obstacles 50 percent greater than its wheel diameter. On another note, the swivel car possesses superior steering capabilities compared to Rocky 7, which cannot steer about a central axis, and hence must change position in order to change its orientation. While the mobile robot MHT possesses excellent climbing capabilities, it requires a control algorithm to retain its posture while climbing steps to avoid tipping over. Furthermore, MHT requires the actuation of twelve joints to perform such motion. On the other hand, the swivel car requires no posture control while climbing a step, is relatively simple to build, and requires the actuation of two joints to climb steps.

Even though our proposed design does not require a complicated control process to climb steps, it needs a rather complicated climbing algorithm which takes into account its platform dynamics and its position with respect to a step.

CHAPTER V

CONCLUSION

In this thesis, we developed kinematic and dynamic models for the steering mechanism of the angular swivel steering platform. We also performed several simulations to validate the steering capability of the platform as well as its energy costs. The performance of the proposed platform was comparable to other step climbing platforms.

Moreover, we captured the effect of the steering action on the position and orientation of the platform by developing a simplified planar model. This planar model in turn allows us to propose a simple step climbing technique. Using this information, we developed a kinematic model to study the robot's planar motion. Due to its design, the robot's planar motion is similar to that of a regular cart-like robot (tricycle robot). This allows us to create a simplified model to study in motion about the ground plane.

Finally, we devised a number of step climbing algorithms based on the mechanical design of the robot. These step climbing procedure can be used as a basis to create more complicated step climbing processes which integrate motion and navigation control.

BIBLIOGRAPHY

- [1] DeSantis, Romano M. "Modeling and path-tracking control of a mobile wheeled robot with a differential drive." *Robotica* 13.04 (1995): 401-410.
- [2] Wilhelm, Alexander, et al. "Dynamics of step-climbing with deformable wheels and applications for mobile robotics." *Intelligent Robots and Systems, 2007. IROS 2007. IEEE/RSJ International Conference on*. IEEE, 2007. Taguchi, Kan. "Enhanced wheel system for step climbing." *Advanced robotics* 9.2 (1994): 137-147.
- [3] Choi, Jin-Kyu, et al. "Passive Step-Climbing Mechanism for a Mobility Aid." *Advanced Robotics* 23.1-2 (2009): 45-64.
- [4] Engelhardt, M., Hildebrand, A., Lange, D., and Schmidt, T. C. (2006). Semantic overlays in educational content networks—the hyIOs approach. *Campus-Wide Information Systems*, 23(4), 254-267.
- [5] Grand, C., BenAmar, F., Plumet, F., and Bidaud, P. (2004, April). Decoupled control of posture and trajectory of the hybrid wheel-legged robot Hylos. In *Robotics and Automation, 2004. Proceedings. ICRA'04. 2004 IEEE International Conference on* (Vol. 5, pp. 5111-5116). IEEE.
- [6] Thomson, T., Sharf, I., and Beckman, B. (2012, May). Kinematic control and posture optimization of a redundantly actuated quadruped robot. In *Robotics and Automation (ICRA), 2012 IEEE International Conference on* (pp. 1895-1900). IEEE.

- [7] Grand, C., Benamar, F., & Plumet, F. (2012). Kinematic Control and Posture Optimization of a Redundantly Actuated Quadruped Robot, 45(3), 477-495.
- [8] Lauria, M., Y. Piguët, and R. Siegwart. "Octopus-an autonomous wheeled climbing robot." Proceedings of the Fifth International Conference on Climbing and Walking Robots. Vol. 322. Suffolk, UK: Professional Engineering Publishing Limited, 2002.
- [9] Volpe, Richard, et al. "The rocky 7 mars rover prototype." Intelligent Robots and Systems' 96, IROS 96, Proceedings of the 1996 IEEE/RSJ International Conference on. Vol. 3. IEEE, 1996.
- [10] Estier, T., et al. "An innovative space rover with extended climbing abilities." Proceedings of Space and Robotics 2000 (2000): 333-339.
- [11] Kimura, H., and Hirose, S. (2002). Development of Genbu: Active wheel passive joint articulated mobile robot. In Intelligent Robots and Systems, 2002. IEEE/RSJ International Conference on (Vol. 1, pp. 823-828). IEEE.
- [12] Kimura, H., Shimizu, K., and Hirose, S. (2004). Development of Genbu: Active-Wheel Passive-Joint Snake-Like Mobile Robot. JOURNAL OF ROBOTICS AND MECHATRONICS., 16, 293-303.
- [13] Lacagnina, M., Muscato, G., & Sinatra, R. (2003). Kinematics, dynamics and control of a hybrid robot Wheeleg. Robotics and Autonomous Systems, 45(3), 1895-1900.
- [14] Shamma, Elie, and Daniel Asmar. "Kinematic analysis of an active angular swivel steering mechanism for robotic mobile bases." Robotics and Biomimetics (ROBIO), 2012 IEEE International Conference on. IEEE, 2012.
- [15] Niku, S. (2010). Introduction to robotics. John Wiley and Sons.
- [16] Ha, Jih-Lian, et al. "Dynamic modeling and identification of a slider-crank mechanism." Journal of sound and vibration 289.4 (2006): 1019-1044.

- [17] Morin, David. Introduction to classical mechanics: with problems and solutions. Cambridge University Press, 2008.
- [18] Otter, Martin, Hilding Elmqvist, and Sven Erik Mattsson. "The new modelica multibody library." Proceedings of the 3rd International Modelica Conference. Linköping), The Modelica Association and Linköping University, 2003.
- [19] Bloch, Anthony M. Nonholonomic mechanics and control. Vol. 24. Springer, 2003.
- [20] Morales, B., and R. Carelli. "Robot control with inverse dynamics and non-linear gains." Latin American applied research 33.4 (2003): 393-397.
- [21] Kamga, A., and Rachid, A. (1996, September). Speed, steering angle and path tracking controls for a tricycle robot. In Computer-Aided Control System Design, 1996., Proceedings of the 1996 IEEE International Symposium on (pp. 56-61). IEEE.
- [22] Siegwart, Roland. Introduction to Autonomous Mobile Robots. Ed. Illah Reza Nourbakhsh. The MIT press, 2004.
- [23] Alexander, J. C., and Maddocks, J. (1990). On the kinematics of wheeled mobile robots. In Autonomous robot vehicles (pp. 5-24). Springer New York.
- [24] Pacejka, Hans. Tyre and vehicle dynamics. Elsevier, 2005.
- [25] Ha, J. L., Fung, R. F., Chen, K. Y., and Hsien, S. C. (2006). Dynamic modeling and identification of a slider-crank mechanism. Journal of sound and vibration, 289(4), 1019-1044.

